Retrogressive thaw slumps temper dissolved organic carbon delivery to streams of the Peel Plateau, NWT, Canada

Cara A. Bulger[1], Suzanne E. Tank[1], and Steven V. Kokelj[2]

[1]Department of Biological Sciences, University of Alberta, Edmonton, AB, T6G 2E9, Canada

[2]Northwest Territories Geological Survey, Government of the Northwest Territories, Yellowknife, NT, X1A 1K3, Canada

Correspondence to: Cara A. Bulger (cara.bulger@gmail.com)

Abstract

In Siberia and Alaska, permafrost thaw has been associated with significant increases in the delivery of dissolved organic carbon (DOC) to recipient stream ecosystems. Here, we examine the effect of retrogressive thaw slumps (RTS) on DOC concentration and transport, using data from eight RTS features on the Peel Plateau, NT, Canada. Like extensive regions of northwestern Canada, the Peel Plateau is comprised of thick, ice-rich tills that were deposited at the margins of the Laurentide Ice Sheet. RTS features are now widespread in this region, with headwall exposures up to 30 m high, and total disturbed areas often exceeding 30 ha. We find that intensive slumping on the Peel Plateau is universally associated with decreasing DOC concentrations downstream of slumps, even though the composition of slump-derived dissolved organic matter (DOM; assessed using specific UV absorbance and slope ratios) is similar to permafrost-derived DOM from other regions. Comparisons of upstream and downstream DOC flux relative to fluxes of total suspended solids suggest that the substantial fine-grained sediments released by RTS features may sequester DOC. Runoff obtained directly from slump rillwater, above entry into recipient streams, indicates that the deepest RTS features, which thaw the greatest extent of buried, Pleistocene-aged glacial tills, release low concentration DOC when compared to paired upstream, un-disturbed locations, while shallower features, with exposures that are more limited to a relict Holocene active layer, have within-slump DOC concentrations more similar to upstream sites. Finally, fine-scale work at a single RTS site indicates that temperature and precipitation serve as primary environmental controls on above-slump and below-slump DOC flux, but that the relationship between climatic parameters and DOC flux is complex for these dynamic thermokarst features. These results demonstrate that we should expect clear variation in thermokarst-associated DOC mobilization across Arctic regions, but that within-region variation in thermokarst intensity and landscape composition is also important for determining the biogeochemical response. Geological and climate legacy shape the physical and chemical composition of permafrost, and thermokarst potential. As such, these factors must be considered in predictions of land-to-water carbon mobilization in a warming Arctic.

1. Introduction

Anthropogenic climate change is significantly affecting the Arctic cryosphere (IPCC, 2014). Temperature increases in circumpolar regions are predicted to be at least 40 % greater than the global mean, while precipitation is also expected to increase significantly in most locations (IPCC, 2014). The resulting degradation of permafrost is forecast to have wide-ranging effects, because thawing has the potential to greatly alter the physical, chemical, and biological functioning of landscapes (Frey and McClelland, 2009; Khvorostyanov et al., 2008a, 2008b; Kokelj et al., 2017b; Schuur et al., 2008, 2013). In particular, permafrost acts as a long term storage medium for solutes and sediments, and as a barrier to the participation of permafrost-sequestered constituents within active biogeochemical cycles (Frey and McClelland 209; Vonk et al. 2015b). Consequently, permafrost thaw can enhance linkages between terrestrial and aquatic systems, via increased transport of terrestrial compounds from land to water (Kokelj et al. 2013; Tanski et al., 2016; Vonk et al., 2015b). Given that circumpolar stores of permafrost carbon are estimated to be almost double that of the atmospheric carbon pool (Hugelius et al., 2014), there is great potential for large increases in carbon mobilization as a result of permafrost thaw (Schuur et al., 2015). Within this context, the mobilization of dissolved organic carbon (DOC) from previously frozen soils is of particular interest, because DOC acts as the primary substrate for the microbially-mediated mineralization of organic carbon to carbon dioxide (Battin et al., 2008), and serves as the primary vehicle for the delivery of terrestrial carbon to the Arctic Ocean (Dittmar and Kattner, 2003; Holmes et al., 2012; Spencer et al., 2015). As a result, the implications of thaw-mediated DOC mobilization may range from effects on the permafrost-carbon feedback, to the ecological and biogeochemical functioning of streams, rivers, and the nearshore ocean (e.g. Fritz et al. 2017; Tank et al., 2012b; Vonk et al., 2015b).

Permafrost thaw can manifest in many different forms, ranging from an increase in active layer thickness and terrain subsidence, to thermokarst features that significantly reconfigure the physical structure of landscapes (Kokelj and Jorgenson, 2013). Of these, thermokarst has the potential to rapidly

62 expose significant quantities of previously-frozen soils to biological and chemical processing (Abbott et
63 al., 2014, 2015; Malone et al., 2013; Tanski et al. 2017). One of the most conspicuous manifestations of
64 thermokarst is the retrogressive thaw slump (RTS; Fig. 1), which develops as a result of mass wasting in
65 ice-rich glacial deposits across northwestern Canada, Alaska, and western Siberia (Kokelj et al., 2017b),
66 and in Yedoma regions of Alaska and Siberia (Murton et al., 2017). Thaw slumps are widespread
67 throughout glaciated terrain in the western Canadian Arctic (Kokelj et al., 2017b; Lantuit et al. 2012),
68 including on the Peel Plateau (Lacelle et al., 2015). These dynamic landforms develop via the ablation of
69 an ice-rich headwall and are particularly efficient at thawing thick zones of ice-rich permafrost and
70 translocating large volumes of sediment from slopes to downstream environments (see Fig. 1). RTS
71 features remain active for decades (Lantuit et al. 2012). They typically stabilize following sediment
72 accumulation at the base of the headwall (Kokelj et al., 2015), but can reactivate causing thaw within
73 the scar zone and upslope expansion of the disturbance (Kokelj et al., 2013; Lantuit and Pollard, 2008).
74 During periods of activity, thawed materials accumulate as a saturated slurry in the slump scar zone (see
75 Fig. 1b) and are transported downslope by mass flow processes, which are accelerated by meltwater-
76 and rainfall-induced saturation (Kokelj et al. 2015). Surface runoff can also remove solutes and
77 suspended sediment from the thawed substrate to downstream environments. Although variation in
78 temperature, precipitation and solar radiation have been correlated with development rates and growth
79 of RTS features (Kokelj et al., 2009, 2013, 2015; Lacelle et al., 2010; Lewkowicz, 1986, 1987), we know
80 little about how these and other environmental drivers might control permafrost-DOC dynamics at the
81 individual-slump to small watershed scale.

82 On the Peel Plateau, an individual thaw slump can impact tens of hectares of terrain, displace
83 hundreds of thousands of cubic meters of sediments, and significantly alter surface water sediment and
84 solute loads (Kokelj et al., 2013; Malone et al., 2013), and thus downstream ecosystems (Chin et al.,
85 2016; Malone et al., 2013). The magnitude of these disturbances and their cumulative impacts is great
86 enough to alter solute loads in the Peel River (70,000 km^2 watershed area; Kokelj et al., 2013), even

though only a small portion of that river's total catchment area (<1%) is influenced by thermokarst (Kokelj et al., 2017b; Segal et al., 2016). This contrasts with many other thaw-affected regions, where increases in solute loads following permafrost disturbance can be transient and have little overall effect on annual solute fluxes (e.g., in High Arctic regions affected by active layer detachments; Lafrenière & Lamoureux, 2013). In addition, permafrost thaw on the Peel Plateau is notable in that it exposes vast quantities of mineral-rich glacial till, which is overlain by a relatively shallow layer of slightly more organic-rich soils (Duk-Rodkin and Hughes, 1992; Kokelj et al. 2017a). Although this till-associated, RTS-susceptible landscape type is found across the Laurentide and Barents-Kara glacial margins of Canada, Alaska, and Siberia (Kokelj et al. 2017b), it contrasts with regions of Alaska and eastern Siberia that are either Yedoma-rich or were covered by patchy or thin drift during the late Pleistocene, and have been a focus for study of permafrost-DOC interactions to date (Abbott et al., 2014, 2015; Drake et al., 2015; Mann et al., 2012; Vonk et al., 2013b).

Thermokarst has been documented to enhance DOC concentrations in recipient aquatic ecosystems in several Arctic regions (Frey and McClelland, 2009; Tank et al., 2012a; Vonk et al., 2013a; Vonk and Gustafsson, 2013). In Alaska, streams affected by thaw slumps have higher DOC concentrations than un-affected systems across various terrain types (2-3 fold increase; Abbot et al., 2014), while in eastern Siberia the DOC concentration in runoff from thawing Yedoma is considerably greater than concentrations in recipient river systems (~30-fold elevation; Spencer et al. 2015). However, multiple factors, including variable carbon content in permafrost soils (Hugelis et al. 2014) and variation in ground ice type and volume (Fritz et al. 2015) may affect DOC release from permafrost. In regions where thermokarst transports fine-grained sediments to aquatic systems, sorption processes may also be important, because dissolved organic matter (DOM) can readily sorb to mineral soils (e.g., Kothawala et al. 2009). Sorption to mineral sediments can cause DOM to be rapidly removed from solution in stream systems (Kaiser and Guggenberger, 2000; Kothawala et al. 2009; McDowell, 1985), while enabling the downstream transport and continued sequestration of organic carbon (Hedges et al.,

1997). This process may be particularly important for regulating DOC dynamics in glacial margin landscapes, where a predisposition to thaw slumping results in an abundance of thermokarst-related slope disturbances which mobilize fine-grained glacial sediment stores to downstream systems (Kokelj et al., 2017a, 2017b; Lantuit et al. 2012; Rampton, 1988). Despite this, we know little about the downstream consequences of permafrost thaw for carbon biogeochemistry in till-dominated glacial landscapes, which are emerging as some of the most geomorphically dynamic permafrost environments in the circumpolar Arctic.

The objective of this study was to quantify how RTS features affect the concentration and composition of DOC across a series of slump-affected streams on the Peel Plateau, and to examine how observed variation in slump morphometry affects DOC dynamics in downstream environments. We further investigated how short-term variation in precipitation, temperature, and solar radiation affect DOC delivery from land to water, using measurements of DOC flux above and below a single RTS feature. We targeted the thermokarst-sensitive Peel Plateau for this work, which is characteristic of till-rich, glacial margin landscapes throughout Canada, Alaska, and Siberia (Kokelj et al. 2017b). By comparing our results to those from elsewhere, we highlight how broad variation in permafrost soil composition, permafrost genesis, and Quaternary history may drive variation in land-freshwater DOC dynamics across divergent regions of the warming circumpolar Arctic.

2 Study Site

2.1 General study site description

Our study was conducted on the Peel Plateau, situated in the eastern foothills of the Richardson Mountains, NWT, Canada, in the zone of continuous permafrost (Fig. 1a). The fluvially-incised Plateau ranges in elevation from 100 to 650 masl. The region was covered by the Laurentide Ice Sheet (LIS) for a brief period (a maximum of 2,000-3,000 years) 18,500 cal yr BP (Lacelle et al., 2013). The bedrock of the

region is Lower Cretaceous marine shale from the Arctic River formation (Norris, 1984) and siltstone overlain by Late Pleistocene glacial, glacio-fluvial and glacio-lacustrine sediments (Duk-Rodkin and Hughes, 1992). These Pleistocene deposits host ice-rich permafrost, overlain by a shallow and commonly organic-rich active layer. Radiocarbon dating in the region has placed the age of relict ground ice in the late Pleistocene (18,100 ± 60 ^{14}Cyr BP; Lacelle et al., 2013). Upper layers of permafrost thawed during the early Holocene and host younger, Holocene-aged organic materials (Lacelle et al., 2013). These are distinguished from deeper Pleistocene-aged permafrost by a thaw unconformity (Burn 1997; Fig. 1), which developed when warmer climate during the early Holocene prompted the thawing of near-surface permafrost. The regional increase in active layer thickness integrated organic matter into the thawed soils and enabling the leaching of soluble ions (see Fig. 1c-d). Climate cooling and permafrost aggradation have archived this notable stratigraphic variation in geochemistry, organic matter content, and cryostructure (Burn 1997; Fritz et al. 2012; Kokelj et al., 2002; Lacelle et al., 2014; Murton and French, 1994).

Ice-marginal glacigenic landscapes such as the Peel Plateau host thick layers of ice-rich sediments, and thus have a predisposed sensitivity to climate-driven thaw slump activity (Kokelj et al., 2017). On the Peel Plateau, slumping is largely constrained by the maximum extent of the LIS, because the thick layers of ice-rich permafrost necessary for RTS activity are typically not present beyond the glacial limits (Lacelle et al., 2015). Fluvial incision provides the topographic gradient necessary for thaw slump development and RTS features are common; ranging in size from numerous small features, to those greater than 20 ha, which are rare (<5% prevalence; Lacelle et al., 2015). The recent intensification of slumping on the Peel Plateau is driven in part by increasing air temperatures and summer rainfall intensity (Kokelj et al., 2015). This intensification is also increasing the thaw of the deepest layer of ice-rich, organic-poor, Pleistocene-aged glacigenic tills that underlie this region. The pattern of abundant thaw slump development across ice-marginal glaciated permafrost landscapes extends from the Peel Plateau across the western Canadian Arctic, and persists at continental scales (Kokelj et al., 2017b).

2.2 Regional climate

The regional climate is typical of the subarctic with long, cold winters and short, cool summers. Mean annual air temperature (1981-2010) at the Fort McPherson weather station (Fig. 1a) is -7.3 ^{o}C with average summer (June-August) temperatures of 13.3 ^{o}C (Environment Canada, 2015). A warming trend of 0.77 ^{o}C per decade since 1970 has been recorded; however these increases are most apparent in the winter months (Burn and Kokelj, 2009). Our sample period spanned the thaw months of July and August; average 1981-2010 temperatures for those months, recorded at Fort McPherson, are 15.2 and 11.8 ^{o}C, respectively, similar to temperatures at Fort McPherson during 2014 (15.6 and 11.6 ^{o}C), but slightly higher than 2014 averages observed at a recently established meteorological station on the Peel Plateau (Fig. 1a; 13.2 ^{o}C in July and 9.5 ^{o}C in August). Annual cumulative rainfall (1981-2010) at Fort McPherson averages 145.9 mm, with July and August having the highest rainfall levels at 46.4 and 39.1 mm (Environment Canada, 2015). In 2014, rainfall for July and August was 71 and 121 mm at Fort McPherson, and 128.7 and 170.7 mm on the Peel Plateau. This continues the trend for this region of increasingly wet summers with numerous extreme rainfall events (Kokelj et al., 2015).

3 Methods

3.1 Slump site selection

Eight RTS features were selected from across the study region, using aerial surveys and previous knowledge of the region (Fig. 1; Fig. S1; Table 1). Selected slumps were characterized by a debris tongue that connected the slump to the valley bottom and directly impacted a stream system. Sampling at each slump occurred at three discrete locations: upstream, within-slump, and downstream of slump influence (Fig. 1b). Upstream sites were trunk streams that connected with the slump flow path further downstream, and were un-affected by any major geomorphic disturbance and thus representative of an undisturbed, pristine environment. Within-slump sampling occurred at points of channelized slump

runoff within the scar zone or upper debris tongue. Downstream sampling locations were below the confluence of the sampled upstream flow and all within-slump runoff paths, and were chosen to be representative of slump impact on aquatic ecosystems across the Peel Plateau landscape. In one instance (Slump HD, August 17), a fluidized flow event between sampling events saturated the scar zone and obliterated within-slump channelized surface flow. As a result, the within-slump sample taken at this site was not representative of typical channelized slump runoff that characterized all other slump sampling conditions, and has been discarded from all analyses.

A general classification of the slumps is difficult as these features are influenced by a diverse range of geomorphic processes that vary in intensity over time (Table 1; Fig. S1). Three of the slumps (FM4, FM2, FM3) are classified as 'mega slumps', characterised by areas greater than 5 ha, a headwall greater than 4 m in height, and a debris tongue that connects the slope to the valley below (Kokelj et al., 2013, 2015). Of these, FM4 possesses a headwall approximately 20 m in height, but was largely stabilized in 2014 (Fig. S1). FM2 is among the largest active slumps in the region, with a headwall 25-30 m high and visible as a much smaller feature in air photos since 1944 (Lacelle et al. 2015). Slump FM3, which was the focus for 'environmental controls' work (further described below), covers an area of approximately 10 ha with a headwall of approximately 10 m height and a debris tongue that extends nearly 600 m down valley (Table 1). Headwall retreat rate at FM3 over a 20 year period has been calculated at 12.5 m yr^{-1} (Lacelle et al., 2015). FM2 and FM3 geochemistry and geomorphology were previously described by Malone et al. (2013). SD is the smallest and youngest slump that we studied, and was initiated when diversion of a small creek caused lateral bank erosion. In 2014, the SD headwall was 2-4 m high with no defined debris tongue and a scar zone extending approximately 20m upslope. The remaining slump sites (HA, HB, HC, HD) were all well-developed active RTS features with headwalls similar to, or smaller than, FM3, but with smaller debris tongues (Table 1). With the exception of SD, slump headwalls exposed permafrost well below a thaw unconformity, indicating that Pleistocene-aged, unweathered glacigenic materials were being thawed (Lacelle et al., 2013).

212

213 *3.2 Field sampling and data collection*

214 3.2.1 The effect of slumping on DOC and stream water chemistry

215 The majority of our sampling was conducted during the summer of 2014. Of the eight slumps
216 that were sampled, three were accessed from the Dempster Highway three times over the sampling
217 season, one (FM3; see also Sect. 3.2.2) was accessed twice from the highway, and four were accessed
218 twice via helicopter (Table 1). At each of the upstream, downstream, and within-slump sampling
219 locations, specific conductivity, pH, and temperature were recorded using a YSI Pro Plus multi-
220 parameter meter. Water samples were collected from directly below the stream surface into 1 L acid
221 washed HDPE bottles and allowed to sit in chilled, dark conditions for 24 h to enable the considerable
222 sediments in these samples to partially settle out of suspension. Sample water was then filtered with
223 pre-combusted (475 ^{o}C, 4 hours) Whatman GF/F filters (0.7 µm pore size). Filtered sample water was
224 transferred into 40 mL acid washed, pre-combusted glass bottles for DOC analysis, or 60 mL acid washed
225 HDPE bottles for the analysis of absorbance and major ions. DOC samples were acidified with
226 hydrochloric acid (1 µL mL^{-1}), following Vonk et al. (2015b). The GF/F filters were retained for analysis of
227 total suspended solids (TSS). Samples for stable water isotopes were collected directly from streams into
228 acid washed 40 mL HDPE bottles with no headspace and sealed. During summer 2016, samples were
229 additionally collected from a subset of slump locations (FM2, FM3, FM4 and SD) for the ^{14}C signature of
230 DOC at upstream and within-slump sites. DO^{14}C samples were collected in acid-washed polycarbonate
231 bottles, allowed to settle for 24 h, and filtered using pre-combusted Whatman GF/F filters into pre-
232 combusted glass media bottles with phenolic screw caps and butyl septa. All samples were refrigerated
233 until analysis. Absorbance samples were analyzed within 1 week of collection, cation samples within 4
234 months of collection, and DOC (including ^{14}C) samples within 1-2 months of collection. Samples for Fe
235 and δ^{18}O were analyzed within 6 months of collection.

236

3.2.2 Environmental controls on DOC flux

To explore how environmental variables control the flux of DOC from RTS-affected streams, we visited slump FM3 an additional 17 times beyond the sampling described above. This intensively-studied site was chosen to be representative of active Peel Plateau slumps that are eroding Holocene- to Pleistocene-aged sediments. During each visit, we measured discharge at the upstream and downstream locations to calculate DOC flux, and collected upstream and downstream DOC concentration samples. Downstream discharge was measured using an OTT C2 current meter at three locations across the small stream and at 40 % depth. Due to the shallow, low flow conditions at the upstream site, upstream discharge was measured using the cross sectional method (Ward and Robinson, 2000). In both cases, discharge was calculated as the product of velocity and stream cross-sectional area. Local daily climate data were obtained from an automated meteorological station established in 2010 by the Government of the Northwest Territories (Kokelj et al. 2015). The station is located within 2 km of slump FM3 (Fig. 1a) and is instrumented for the measurement of air temperature, rainfall, and net radiation.

3.3 Laboratory analyses

3.3.1 Major ions, dissolved organic carbon, $\delta^{18}O$ and $DO^{14}C$

Cation concentrations (Ca^{2+}, Mg^{2+}, Na^{+}) were analyzed on a Perkin Elmer Analyst 200 Atomic Absorption Spectrometer at York University. A subset of collected samples were analyzed for total dissolved Fe at the University of Alberta on an Inductively Coupled Plasma - Optical Emission Spectrometer (Thermo Scientific ICAP6300), to allow for the correction of our Specific UV Absorbance results (see below). DOC samples were analyzed on a Shimadzu TOC-V analyzer; DOC was calculated as the mean of the best 3 of 5 injections with a coefficient of variation of <2%; the precision of a 10 mg L^{-1} caffeine standard across all sample runs was 0.32 mg L^{-1}. A Picarro liquid water isotope analyzer was used to measure $\delta^{18}O$ at the University of Alberta, following filtration (0.45 µm cellulose acetate, Sartorius) into 2 mL autosampler vials (National Scientific), without headspace. The precision of our

$\delta^{18}O$ analysis is ± 0.2 ‰. The radiocarbon signature of DOC was measured following extraction and purification at the A.E. Lalonde AMS facility (University of Toronto) using a 3MV tandem accelerator mass spectrometer (High Voltage Engineering) following established methodologies (Lang et al., 2016; Palstra and Meijer, 2014; Zhou et al., 2015), and is reported with an error estimate of 1σ.

3.3.2 Total suspended solids

Samples for TSS were filtered in the field for later analysis, ensuring that there was enough sediment on the pre-combusted (475 ^{o}C, 4 hours) and pre-weighed GF/F filters. Filters were stored frozen, dried at 60 ^{o}C for 8 hours, placed in a desiccator overnight and promptly weighed. TSS was calculated as the difference in filter weight before and after sediment loading, divided by volume filtered.

3.3.3 Dissolved organic matter spectral characteristics

DOM composition was assessed using absorbance-based metrics. A 5 cm quartz cuvette was used to obtain UV-visible spectra data from 250-750 nm, using a Genesys 10 UV-Vis spectrophotometer. A baseline correction was applied to eliminate any minor interference from particles < 0.7 µm (Green and Blough 1994). Specific UV absorbance at 254 nm ($SUVA_{254}$), which is correlated with DOM aromaticity (Weishaar and Aiken, 2003), was calculated by dividing the decadal absorbance at 254 nm (m^{-1}) by the DOC concentration (mg L^{-1}). $SUVA_{254}$ values were corrected for Fe interference following Poulin et al. (2014) using maximum Fe concentrations from laboratory analyses or as reported in Malone et al. (2013). Spectral slopes between 275 and 295 nm, and 350 and 400 nm ($S_{275-295}$, $S_{350-400}$) were calculated following Helms et al. (2008), and are reported as positive values to adhere to mathematical conventions. Slope ratios (S_R), which correlate with DOM molecular weight (Helms et al., 2008), were calculated as the ratio of $S_{275-295}$ to $S_{350-400}$.

3.4 Statistical analyses and calculations

Statistical analyses were completed in R version 3.1.3 (R Core Team, 2015) using packages 'nlme' (Pinheiro et al., 2015), 'lmtest' (Zeileis and Hothorn, 2002), 'lmSupport' (Curtin, 2015), 'car' (Fox and Weisberg, 2011), and 'zoo' (Zeileis and Grothendieck, 2005). The effect of slumping on stream chemistry and optical characteristics was assessed using linear mixed effects models in the 'nlme' package of R. For each parameter, analyses were split into two separate models that included data for upstream and downstream chemistry, and upstream and within-slump chemistry. We used this approach to separately assess the effects of slumping downstream of slump systems, and to compare the composition of slump runoff to nearby, pristine environments. For each analysis, we included slump location (see Table 1) as a random effect, and considered models that either nested Julian date within the random effect of slump location, or allowed Julian date to occur as a fixed effect. The best model was chosen using the Akaike Information Criterion (AIC), and best-fit models were refit with a variance structure to ensure that model assumptions were met. The variance structures varIdent (for within-slump site and slump location) and varFixed (for Julian date) were used together (using varComb) and in isolation for this purpose (Zuur et al., 2009). AIC values for the weighted and un-weighted models were again compared to choose a final model of best fit for each analysis.

We used the high-frequency data from slump FM3 to assess how environmental conditions (rainfall, temperature, solar radiation) and TSS affect DOC delivery to slump-affected streams. To do this, we conducted multiple linear regressions, using AIC values to determine models of best fit (Burnham and Anderson, 2002). To enable a specific assessment of environmental controls on downstream DOC flux, upstream DOC flux was separated out into a distinct regression analysis, because upstream DOC flux was strongly correlated with flux downstream, and therefore overwhelmed all environmental variables in the downstream model. Models were tested for serial correlation using the auto-correlation function, and models with variance inflation factors greater than 10 or significant Durbin Watson test results (indicative of correlated variables; Durbin & Watson, 1950; Hair et al., 1995)

were discarded. Residuals were examined to ensure the model was a good fit for the data (Zuur et al., 2009). We considered both time-of-sampling (0 h) and past (48, 72, and 120 h) environmental conditions in our analyses. Because cumulative values for environmental variables (i.e. accumulated rainfall in the previous 48, 72 and 120 h) showed a strong positive correlation to one another, we used temporally shifted data (i.e. rainfall 48, 72 and 120 h prior to the DOC flux measurement) in the final model. Similar models were also constructed to examine the effects of environmental drivers on DOC concentration. Differences in paired upstream-downstream measures of DOC flux and concentration at slump FM3 were also assessed using a Wilcoxon Signed Rank Test, a non-parametric analog to the paired-t test.

Following our finding of decreasing DOC concentrations downstream of slumps (see Sect. 4.1 and 5.1) we used data from slump FM3, where we have upstream, downstream, and within-slump DOC concentration measurements, and upstream and downstream discharge measurements, to calculate a mass balance for DOC across the three sampling locations. These data – available for all three locations on two dates during the summer of 2014 – were used to calculate DOC flux at upstream and downstream sites as $flux_{DOCdown} = [DOC]_{down} \bullet discharge_{down}$ or $flux_{DOCup} = [DOC]_{up} \bullet discharge_{up}$, and at within-slump sites as $flux_{DOCwithin} = [DOC]_{within} \bullet (discharge_{down} - discharge_{up})$. We calculate a similar mass balance for TSS, which we use as a rough tracer for the inflow of slump runoff over the < 1 km span between upstream and downstream locations at this site.

4. Results

4.1 DOC concentration across slump sites

While DOC concentrations ranged broadly across pristine streams on the Peel Plateau (Fig. 2; from 5.4 to 26.1 mg L^{-1} at upstream, pristine sites), concentrations consistently declined downstream of slumps, when compared to paired, upstream locations ($p<0.001$; Fig. 2; Table 2). Although this effect was modest (typically less than 20 %; Fig. 2), it occurred reliably across all slump sites. In contrast, comparisons of upstream and within-slump sites showed no consistent trend in DOC concentration,

when evaluated across all slump locations (p=0.153; Fig. 2; Table 2). Instead, the effects of slumping on the DOC concentration of slump runoff varied by site. At the largest, most well-developed slump complexes (FM4, FM2, and FM3), where debris tongues are extensive and thaw extends well into the deepest layer of Pleistocene-aged glacigenic materials, DOC concentrations tended to be lower in slump runoff than at the paired upstream sites (Fig. 2). At more modestly-sized slumps (HB, HC, and HD), where modern and relict Holocene active layers comprise a greater proportion of thawed materials, within-slump DOC concentrations tended to be higher than values upstream (Fig. 2). Within each site, DOC concentrations were relatively consistent across the 2-3 sampling periods (Fig. 2).

4.2 Bulk chemistry of pristine waters and slump runoff

To better understand how the input of slump runoff affects downstream DOC, we examined concentrations of major ions, conductivity and TSS as 'tracers' of slump activity, because these constituents have previously been shown to be significantly affected by slumping in this region (Kokelj et al., 2005, 2013; Malone et al., 2013; Thompson et al., 2008). Major ion (Ca^{2+}, Mg^{2+}, Na^{+}) concentrations in slump runoff were considerably greater than in pristine streams (a 2.7 to 11.7-fold increase; Fig. 3b-d; Table 2). These patterns were similar, though muted, at slump-affected downstream sites, where major ion concentrations were 1.5 to 3.5-fold greater than at pristine sites (Fig. 3b-d; Table 2). Mean conductivity also increased significantly as a result of slumping ($p< 0.001$; Table 2): within-slump sites had conductivity values that were 9.2-fold greater than upstream sites, while downstream values were an average of 2.6 times greater than those upstream (Fig. 3e). Finally, TSS was also significantly elevated at slump-affected sites ($p< 0.001$; Table 2) with concentrations being more than two orders of magnitude greater within slumps, and more than one order of magnitude greater downstream, when compared to upstream sites (Fig. 3a). The effect of slump runoff on downstream chemistry is also reflected in DOC: ion, and DOC: TSS ratios, which decreased markedly between upstream and downstream locations. For example, molar ratios of (Ca^{2+} + Mg^{2+}): DOC averaged 0.78 ± 0.37 (mean ±

362 standard error) upstream of slumps, but 2.07 ± 0.45 downstream, while average gram-weight ratios of
363 TSS: DOC were 32 ± 12 upstream, but 1454 ± 332 at downstream locations.
364
365 *4.3 Spectral and isotopic characteristics*
366 $SUVA_{254}$, which is positively correlated with DOM aromaticity (Weishaar and Aiken, 2003), was
367 significantly lower within slumps, and downstream of slumps, than in upstream, pristine, environments
368 ($p<0.001$; Fig. 4; Table 2). Mean within-slump $SUVA_{254}$ was less than half of that observed for pristine
369 waters (Fig. 4), while downstream values declined by approximately 20 %. In accordance with the
370 $SUVA_{254}$ results, $S_{275-295}$, $S_{350-400}$, and S_R were all significantly greater within slumps when compared to
371 upstream sites ($p<0.001$; Fig. 4; Table 2), indicating lower DOM molecular weight within slumps (Helms
372 et al., 2008). Differences in slope parameters between upstream and downstream locations were muted
373 relative to the within-slump: upstream comparisons (Fig. 4), with $S_{275-295}$ ($p=0.011$) and S_R ($p<0.001$)
374 increasing significantly, but more modestly, downstream of slumps, and $S_{350-400}$ declining slightly
375 ($p=0.001$; Fig. 4; Table 2).
376 Upstream $\delta^{18}O$ averaged -20.1 ‰ ± 0.12, which corresponds to a modern active-layer pore
377 water $\delta^{18}O$ signature for this region (Lacelle et al., 2013; Fig. 5). Within-slump $\delta^{18}O$ was discernibly
378 depleted when compared to upstream locations, with mean values of -22.7‰ ± 0.72, which falls
379 between previously-identified regional endmembers for Pleistocene-aged ground ice (18,100 ± 60 ^{14}Cyr
380 BP) and the modern active layer (Lacelle et al., 2013; Fig. 5). Within-slump $\delta^{18}O$ was also much more
381 variable between RTS features than upstream and downstream $\delta^{18}O$ values. Similar to upstream sites,
382 downstream $\delta^{18}O$ clustered near the modern active layer $\delta^{18}O$ endmember, but with a small depletion
383 that was consistent with a contribution from slump inflow (-20.7‰ ± 0.21).
384 To further investigate the effect of water source on DOM composition, we examined the
385 relationship between $SUVA_{254}$ and $\delta^{18}O$. More depleted samples taken from within-slump sites had
386 clearly depressed $SUVA_{254}$ values when compared to samples with more enriched $\delta^{18}O$ (Fig. 5). Of the

large, most well-developed slumps that were identified in Sect. 4.1, two (FM2 and FM3), in addition to site HB, had $\delta^{18}O$ values that were more depleted than the Holocene-aged icy diamicton values reported in Lacelle et al. (2013), suggesting some contribution of runoff from older, Pleistocene-aged permafrost (Fig. 5). It is likely that the $\delta^{18}O$ signal at the relatively stable mega-slump site (FM4) was somewhat diluted by the 7.2 mm of rainfall that fell in the 48 hours preceding our sample. Although sites FM3 and SD received 12.4 and 3.5 mm of rain, respectively, in the 48 hours prior to sampling, these are both much more active slump sites, and thus less prone to dilution of the slump outwash signature. There was no significant rainfall immediately preceding sampling at any other sites.

The radiocarbon signature of DOC from upstream and within-slump locations at sites FM4, FM2, FM3, and SD largely mirrors the $\delta^{18}O$ results. DOC from sites upstream of slump disturbance was approximately modern in origin (ranging from 217 ± 24 ^{14}C yr BP to modern in age; Table 3). In contrast, within-slump waters from site FM2 and FM3 were early Holocene-aged (9592 ± 64, and 8167 ± 39 ^{14}C yr BP, respectively; Table 3). Slump runoff from site SD was older than at upstream sites, but younger than for the larger slumps, described above (1157 ± 23 ^{14}C yr BP; Table 3).

4.4 Patterns and environmental drivers of DOC flux

Similar to our findings for the distributed sampling scheme (Fig. 2), downstream DOC concentration was consistently lower than concentrations upstream, across the 19 paired measurements taken at the intensively studied site FM3 ($p<0.001$, N=19, W=0; Wilcoxon Signed Rank Test; mean decline of 2.5 ± 0.2 mg L^{-1}, compared to a mean upstream concentration of 13.6 ± 0.5 mg L^{-1}). To explore environmental drivers of DOC movement within this landscape, however, we focus on DOC flux, which allows a direct assessment of slump-mediated DOC addition to this system. Downstream DOC flux (mg s^{-1}) tended to be slightly greater than upstream flux on most, but not all, sampling occasions (Fig. 6). As a result, paired comparisons indicate no statistical difference between upstream and downstream DOC flux at this site (Wilcoxon signed rank test; $p=0.096$, N=19, W=53).

412 Because upstream and downstream DOC flux were strongly correlated to one another (r^2 = 0.94;
413 $p<0.0001$), our downstream model was run without upstream DOC flux as a predictor variable. The best-
414 fit multiple linear regression model for downstream DOC flux (r^2 = 0.84; $p<0.01$) retained seven
415 variables, of which two were significant (Table 4). Of these, air temperature (72 h prior to sampling)
416 showed a negative relationship with downstream DOC flux while rainfall (0 h; time of sampling) showed
417 a strong positive relationship (Table 4). The best-fit model for upstream DOC flux (r^2 = 0.87; $p<0.001$)
418 also retained seven variables, of which four were significant ($p<0.05$; Table 4). Similar to the
419 downstream analysis, air temperature (0 h, 72 h) displayed a negative relationship, and time-of-
420 sampling (0 h) rainfall a strong positive relationship, with DOC flux (Table 4). However, 120 h rainfall
421 showed a negative relationship with DOC flux in this model. Regressions assessing controls on
422 downstream DOC flux relative to upstream flux (i.e., as a ratio, or the difference between the two
423 values) were not significant. Models to explore controls on upstream and downstream DOC
424 concentration were also relatively similar to one another, showing strong, positive relationships
425 between DOC concentration and air temperature, and more modest negative relationships between
426 DOC concentration and net radiation (Table 4).
427
428
429 **5. Discussion**
430 *5.1 Retrogressive thaw slumps and carbon delivery to streams of the Peel Plateau*
431 In both Eastern Siberia (Spencer et al. 2015; Vonk et al., 2013b) and Alaska (Abbott et al., 2014)
432 permafrost slumping has been associated with significant increases in DOC mobilization from terrestrial
433 to aquatic systems. Our data show that this was not the case on the Peel Plateau, where the landscape-
434 induced variation in DOC concentration among pristine stream sites was much greater than the change
435 in stream water DOC as a result of slumping. Across all of our study sites, DOC concentrations
436 consistently declined downstream of slumps when compared to upstream locations, while at an

intensively-sampled slump, DOC flux did not differ significantly between upstream and downstream locations. In contrast, comparisons of channelized slump runoff (our within-slump sites) and paired un-affected sites showed no consistent DOC trend. Instead, DOC concentrations in slump runoff were either greater than, or less than, their comparison upstream locations, in a manner that differed depending on slump morphological characteristics such as slump size and headwall height (Fig. 1; see further discussion in Sect. 5.3). The moderate effect of slumping on DOC concentration occurred despite the significant influence of these disturbances on the delivery of many biogeochemical constituents to recipient streams. For example, conductivity was approximately one order of magnitude greater, and TSS two orders of magnitude greater, in slump-derived runoff than at upstream, un-affected sites. This led to substantially increased TSS:DOC and (Ca + Mg):DOC ratios downstream of slumps, when compared to pristine, upstream locations.

Decreasing DOC concentrations downstream of slumps, despite increasing concentrations of indicators of slump activity (major ions, TSS) could be driven by several, potentially co-occurring mechanisms. In some locations, decreases may be partially caused by low DOC concentrations in slump outflow (a dilution effect; see slumps FM2, FM3, and FM4 in Fig. 2; further discussed in Sect. 5.3). However, our results suggest that DOC sorption to suspended inorganic sediments could also play a role in regulating DOC dynamics in slump-affected systems. At multiple sites (HB, HC, and HD), DOC concentrations declined downstream of slumps despite a modest elevation in DOC concentration in slump drainage waters (Fig. 2). Thermokarst contributes significant amounts of fine-grained glacigenic sediment to fluvial systems on the Peel Plateau (Kokelj et al., 2013; silty-clay sediment classification for FM3 in Lacelle et al., 2013). DOC sorption can occur in seconds to minutes in freshwater systems (Qualls and Haines, 1992), with fine-grained materials being particularly conducive to this process (Kothawala et al., 2009). Data from site FM3, where we have upstream and downstream discharge data coupled with DOC and TSS concentrations at upstream, downstream, and within-slump locations on two separate dates, allows possible DOC sorption to be assessed. On these dates, DOC flux declined downstream of

462 the slump (i.e., $flux_{DOCdown} < flux_{DOCup}$), despite a clear and measurable efflux of DOC from the slump to
463 the receiving stream system ($flux_{DOCwithin}$; Fig. 7). This same calculation using TSS as a rough tracer of
464 slump inflow shows the calculated efflux of TSS from this slump ($flux_{TSSwithin}$) to be almost identical to the
465 increase in TSS flux downstream of the disturbance (as $flux_{TSSdown} – flux_{TSSup}$; Fig. 7). Thus, it seems likely
466 that relatively rapid processes, such as sorption to mineral surfaces, are affecting DOC dynamics in
467 thermokarst-affected fluvial systems on the Peel Plateau.

468 Although a similar decrease in DOC concentration with slumping has been found for lakes in this
469 region (Kokelj et al., 2005), our findings contrast with those from other previously-studied areas of the
470 Arctic, where thermokarst leads to an efflux of high-DOC waters from slump features (e.g., Abbott et al.,
471 2014; Vonk et al., 2013a). However, ice-marginal glaciated landscapes are common throughout the
472 western Canadian Arctic, and in many other Arctic regions. The thick, mineral-rich, carbon-poor tills with
473 high ice contents that characterize these landscapes is predisposed to intense thaw slumping and the
474 mobilization of glacigenic sediments from slope to stream (Kokelj et al., 2017b). As a result, DOC
475 'sequestration' following slumping seems unlikely to be limited to the Peel Plateau. Given the high TSS
476 export and apparent organic carbon sorption to glacigenic sediments observed with slumping on the
477 Peel Plateau, we expect that substantial organic carbon is mobilized from these disturbances in the
478 particle-attached, rather than dissolved, form (i.e., as particulate organic carbon; POC). Quantifying this
479 POC mobilization and fate once subject to contemporary biogeochemical processing, and the
480 mechanisms that enable DOC sequestration to occur, are key avenues for future research on the Peel
481 Plateau and elsewhere.

482

483 *5.2 The effect of retrogressive thaw slumps on DOM composition*

484 Although DOC concentrations did not increase in RTS-affected streams, absorbance metrics
485 clearly indicate that slump-derived DOM on the Peel Plateau is compositionally different than DOM from
486 upstream locations. Upstream waters had significantly higher $SUVA_{254}$ values than downstream and

487 within-slump sites (Table 2, Fig. 4). Similarly, while the average S_R of Peel Plateau upstream waters (0.74
488 ± 0.005) was within the range of S_R typically associated with fresh, terrestrial DOM (~ 0.70; Helms et al.,
489 2008), values were significantly greater within-slump (0.92 ± 0.015) and downstream (0.89 ± 0.009)
490 (Table 2, Fig. 4), indicating decreasing DOM molecular weight as a result of RTS activity. High $SUVA_{254}$
491 values accompanied by low S_R at upstream sites suggest that water flow in undisturbed catchments is
492 restricted to shallow, organic-rich flowpaths through the active layer, with permafrost inhibiting water
493 contributions from deeper, groundwater or mineral-associated sources (Balcarczyk et al., 2009;
494 MacLean et al., 1999; Mann et al., 2012; O'Donnell et al., 2010; Street et al. 2016). In contrast, within-
495 slump and downstream measurements indicate a clear transition in DOM source.
496 The comparatively low $SUVA_{254}$, and high S_R values for downstream and within-slump sites
497 indicate that permafrost-derived carbon on the Peel Plateau is characterized by relatively low molecular
498 weight and aromaticity, and is thus similar in its composition to permafrost carbon from other regions.
499 For example, $SUVA_{254}$ values were low in waters draining active thaw slumps when compared to
500 stabilized and undisturbed sites on the North Slope of Alaska (Abbott et al., 2014), while in Siberia, ^{14}C-
501 depleted DOM from small tributary streams affected by thermokarst had lower $SUVA_{254}$ values
502 compared to younger DOM from the Kolyma River mainstem (Mann et al., 2015; Neff et al., 2006).
503 Although $SUVA_{254}$ values for waters draining Peel Plateau thaw slumps are slightly lower than those
504 reported for Siberian Yedoma disturbances (Mann et al., 2015), the overall similarity of permafrost-
505 derived DOM composition across these various regions is striking, given the regional differences in
506 permafrost origin and landscape history. For example, the DOM released by permafrost thaw on the
507 Peel Plateau is till-associated, and early-Holocene in mean age, while east Siberian Yedoma is composed
508 of loess-derived Pleistocene deposits that sequestered carbon in association with synengetic permafrost
509 aggradation. This suggests that common processes may enable the organic matter contained in
510 permafrost soils to become compositionally similar across diverse Arctic regions. Such compositional
511 similarity also indicates that permafrost-origin DOM from the Peel Plateau – similar to that from other

512 regions (Abbott et al., 2014; Drake et al., 2015) – may be readily degraded by bacteria, despite the
513 divergent origin of this carbon.
514
515 *5.3 The effect of slump morphometry on runoff water biogeochemistry*
516 $\delta^{18}O$ and $DO^{14}C$ data provide further evidence that intense slumping enables novel sources of
517 water and solutes to be transported to fluvial systems on the Peel Plateau. For most of the RTS features
518 that we studied, the $\delta^{18}O$ signature of within-slump waters ranged from similar to the 'icy diamicton'
519 that overlies the early Holocene thaw unconformity, to that for underlying Pleistocene-aged ground ice
520 (Lacelle et al., 2013; Fig. 5). Similarly, $DO^{14}C$ from a subset of sites indicates slump-derived DOC is early
521 Holocene in age for all but the shallowest slump surveyed. This suggests that our slump outflow samples
522 were likely comprised of a mixture of Pleistocene-, Holocene-, and modern-sourced water (see Fig. 1c-
523 e), but that the contribution of these end-members varied across slumps depending on the relative
524 volume of different stratigraphic units being mobilized.
525 The between-site variation in $\delta^{18}O$ signature (Fig. 5) and relative DOC concentration (Fig. 2b) of
526 slump runoff waters appears to be related to differences in slump morphometry (size, headwall height,
527 and the length and area of the debris tongue; see Table 1 and Fig. 1c-e) across sites. The well-developed,
528 larger slump complexes (FM4, FM2 and FM3) were more likely to have $\delta^{18}O$ signatures that lie between
529 end-member values for Holocene-aged icy diamicton and Pleistocene-aged ground ice (Fig. 5; although
530 note that dry and stabilized FM4 differs somewhat from this trend). These well-developed slumps also
531 stood out as displaying within-slump DOC concentrations that were lower than at upstream comparison
532 sites (Fig. 2b). The headwall exposure at these largest slumps exposes Pleistocene-aged permafrost to
533 several m depth (see Fig. 1c), while the evacuation of scar zone materials have produced extensive
534 debris tongues up to several km long (Table 1, Figs. 1b, S1e and S1g). This significant exposure of
535 mineral-rich, Pleistocene-aged glacial till contributes solutes from low-carbon mineral soils and low-DOC
536 ground ice (Fritz et al. 2015; Tanskii et al. 2016) to runoff, while entraining fine-grained sediments which

provide mineral surface area for possible DOC adsorption. Adsorption may be further enhanced as slump and stream runoff continue to entrain sediments as flows incise the lengthy debris tongue deposits. In contrast, slumps with slightly shallower headwalls (HA, HB, HC, HD; see Fig. 1d), and less well-developed debris tongues (Table 1), appear to elicit a slightly different response than the largest slumps discussed above. At these mid-sized sites, within-slump DOC concentrations were typically higher than those found at upstream comparison sites (Fig. 2b), which may reflect the greater relative inputs from thawing of the Holocene-aged relict active layer, and decreased interaction with debris tongue deposits at these smaller disturbances. Similarly, runoff $\delta^{18}O$ tends to lie between Holocene and modern end-member values at these sites (though note the more depleted value for HB; Fig. 5), indicating a lower relative contribution of Pleistocene-aged ground ice to slump outflow waters.

Finally, the youngest and shallowest slump surveyed (SD), exposed only near-surface permafrost soils for leaching and geochemical transport (Figs. 1e and S1; Table 1), and not the underlying mineral and ice-rich glacigenic substrates. Accordingly, the effects of slumping on stream chemistry, optical parameters, and isotopes were muted at SD when compared to the larger slumps discussed above. These morphometry-related shifts in the downstream effects of slumping suggest that we should expect non-linearity in the biogeochemical response as RTS features develop over time, particularly if slumping continues to intensify with future warming on the Peel Plateau (e.g., Kokelj et al., 2017b), underscoring the importance of long-term monitoring on the Peel Plateau and elsewhere.

5.4 Environmental controls on DOC flux and concentration

Air temperature and rainfall exerted the strongest control on DOC flux at our intensively studied site, which was chosen to be representative of active Peel Plateau slumps that eroding Holocene- to Pleistocene-aged sediments (slump FM3; Fig. 6; Table 4). Upstream of the slump, rainfall was positively correlated, and air temperature negatively correlated, with DOC flux. However, precipitation events were negatively related to temperature (Fig. 6), suggesting that over a single season, precipitation

562 served as the primary environmental control on upstream DOC flux. DOC concentration was relatively
563 constant with upstream discharge ($r=-0.342$, $p=0.151$), indicating that precipitation controlled DOC flux
564 largely as a result of changes in runoff, and that DOC was not source-limited over the time scale of our
565 investigation. However, upstream DOC concentration was positively related to temperature (Table 4),
566 suggesting a link between biological activity and within-soil DOC production (c.f. Pumpanen et al., 2014).
567 These upstream-of-slump results are consistent with work from other undisturbed permafrost and
568 boreal regions, where precipitation and catchment runoff have been shown to control DOC flux in
569 streams (Prokushkin et al., 2005; Pumpanen et al., 2014), and increasing temperature has been shown
570 to increase DOC production in soils (Christ and David, 1996; Neff and Hooper, 2002; Prokushkin et al.,
571 2005; Yanagihara et al., 2000). They are also consistent with the concept that the permafrost barrier
572 forces runoff to travel through the shallow active layer, where high hydraulic conductivity leads to rapid
573 transport of carbon into fluvial systems (O'Donnell et al., 2010; Striegl et al., 2005).
574 Slumping did not significantly affect downstream DOC flux at the intensively studied slump site,
575 when compared to DOC flux upstream (Fig. 6; Sect. 4.4). Although concentration consistently declined
576 downstream at FM3 (Sect. 4.1 and 4.4), downstream DOC flux was either slightly higher, or slightly
577 lower, than upstream flux; a result that seems likely to play out at other, comparable Peel Plateau
578 slumps, given the coherent concentration patterns that we observed across this landscape. Concordant
579 with the lack of slump effect on DOC flux, neither the ratio of (downstream: upstream) or difference
580 between (downstream – upstream) upstream and downstream DOC flux could be explained by any of
581 our environmental variables, while the environmental controls on downstream flux were almost
582 identical to those upstream (Table 4). The lack of clear environmental control on relative downstream:
583 upstream DOC flux occurred despite the fact that precipitation has been shown to be a strong driver of
584 sediment movement from slump features on the Peel Plateau, at time scales similar to those used for
585 this work (Kokelj et al., 2015).
586 Considering the Peel Plateau landscape as a whole, it appears that precipitation serves as a

primary, positive control on DOC flux. Thus, this study adds DOC production to the list of changes – such as increasing slump activity and sediment mobilization – that can be expected with the increased precipitation that is affecting this region, and is predicted for many Arctic locations (IPCC, 2014; Kokelj et al., 2015). However, it appears that slumping does not over-ride the landscape-scale control on DOC flux in this system – at least at the scale of this single-season – perhaps because processes like DOC sorption mask the influx of slump-derived DOC (Fig. 6). This result highlights the complexity of the interaction between changing climatic parameters and DOC dynamics on the Peel Plateau, where thaw slumps of increasing size mobilize till, glaciolacustrine, glaciofluvial, and organic deposits, while also draining contemporary active layers across a shrub-tundra to spruce forest upland gradient. DOC dynamics are thus affected by both water and carbon generation across these variable landform types, and by biogeochemical interactions such as mineral adsorption in recipient systems. Future work to tease apart the interactions between changing climatic parameters, slump development, and resultant biogeochemical effects is clearly warranted, with the recognition that environmental controls on slump activity, and thus downstream biogeochemistry, can be expected to show marked regional variation (see for example, work from Eureka Sound; Grom & Pollard 2008).

6. Conclusions: Dissolved carbon mobilization across diverse permafrost landscapes

Carbon dynamics in Arctic aquatic systems are influenced by numerous factors, including geology, Quaternary and glacial history, soil composition, vegetation, active layer dynamics, and the nature and intensity of thermokarst. As a result, the effect of permafrost thaw on DOC concentration and flux should – at a fundamental level – vary across broad, regional scales. Our results demonstrate that we can expect marked inter-regional variation in DOC transport to streams in response to permafrost degradation. For example, declines in DOC concentration downstream of slumps on the Peel Plateau clearly differ from what has been found in eastern Siberia and regions of Alaska, where thermokarst releases substantial quantities of DOC (e.g., Spencer et al. 2015), and increases DOC

612 concentrations in downstream systems (Abbott et al. 2015). Efforts that incorporate information
613 concerning the geology and Quaternary history of thawing landscapes, the physical and geochemical
614 composition of permafrost soils, and the nature and intensity of thermokarst processes within
615 landscapes (see, for example, Olefeldt et al. 2016) will considerably increase our ability to predict
616 climate-driven changes in carbon delivery from land to water on a pan-Arctic scale.

617 At finer scales, this work underscores the variability of thermokarst effects within regions, and
618 the local-scale control on this variability. On the Peel Plateau, between-site differences in the
619 biogeochemical effect of thermokarst are related to variation in soil stratigraphy (i.e., the relative depth
620 of the Holocene-aged paleo-active layer) and ever-evolving slump morphometry. Although striking
621 within-region variability in biogeochemical response to thermokarst has been seen elsewhere (e.g.,
622 Watanabe et al., 2011), responses in other regions occur as a result of very different – and region-
623 specific – landscape-level drivers. This landscape-specificity also extends to the non-linear
624 biogeochemical response as thermokarst features develop over time. Changes in downstream
625 biogeochemistry with slump development are very different on the Peel Plateau, for example, than in
626 other regions (e.g., Abbot et al. 2015), while temporal non-linearity can also be expected for other types
627 of permafrost thaw (Kokelj et al. 2002, Vonk et al. 2016) such as increasing active layer thickness
628 (Romanovsky et al. 2010). It seems clear that a tiered approach, targeted within regions to understand
629 local controls on thaw-driven DOC mobilization, and across regions to document the effects of broad-
630 scale variation imposed by geological and climate legacy, is required to understand future
631 biogeochemical functioning of thermokarst-affected landscapes in a warming circumpolar Arctic.
632
633

Data availability: Data associated with this manuscript have been made available in Tables S1 and S2.

Competing interests: The authors declare that they have no conflict of interest.

Acknowledgements

Financial support for this research was provided by Ontario Graduate Scholarship, York University Fieldwork Cost Fund, York University Research Cost Fund, Northern Scientific Training Program, NSERC Discovery and Northern Research Supplement grants to SET, the Campus Alberta Innovates Program, and the Polar Continental Shelf Program. We would like to thank Scott Zolkos for his support as a field assistant and for the production of Figure 1; S. Tetlichi, D. Neyando, and P. Snowshoe for field sampling assistance; and the Tetlit Gwich'in (Fort McPherson) Renewable Resources Council. Sarah Shakil and Scott Zolkos assisted with the collection of samples for $DO^{14}C$; Justin Kokoszka performed geospatial calculations of slump area and debris tongue length. Comments from Michael Fritz and one anonymous reviewer greatly improved the content of the manuscript. NWT Geological Survey contribution number xxxx.

650 **Literature Cited**

651 Abbott, B. W., Larouche, J. R., Jones, J. B., Bowden, W. B., and Balser, A. W.: Elevated dissolved organic
652 carbon biodegradability from thawing and collapsing permafrost, J. Geophys. Res., 119, 2049–2063,
653 doi:10.1002/2014JG002678, 2014.

654 Abbott, B. W., Jones, J. B., Godsey, S. E., Larouche, J. R., and Bowden, W. B.: Patterns and persistence of
655 hydrologic carbon and nutrient export from collapsing upland permafrost, Biogeosciences, 12,
656 3725–3740, doi:10.5194/bg-12-3725-2015, 2015.

657 Balcarczyk, K. L., Jones, J. B., Jaffé, R., and Maie, N.: Stream dissolved organic matter bioavailability and
658 composition in watersheds underlain with discontinuous permafrost, Biogeochemistry, 94, 255–270,
659 doi:10.1007/s10533-009-9324-x, 2009.

660 Battin, T. J., Kaplan, L. A., Findlay, S., Hopkinson, C. S., Marti, E., Packman, A. I., Newbold, J. D., and
661 Sabater, F.: Biophysical controls on organic carbon fluxes in fluvial networks, Nat. Geosci., 1, 95–100,
662 doi:10.1038/ngeo101, 2008.

663 Burn, C. R.: Cryostratigraphy, paleogeography, and climate change during the early Holocene warm
664 interval, western Arctic coast, Canada. Can. J. Earth Sci. 34, 912-925, doi: 10.1139/e17-076, 1997.

665 Burn, C. R. and Kokelj, S. V: The environment and permafrost of the Mackenzie Delta area, Permafr.
666 Periglac. Process., 20, 83–105, doi:10.1002/ppp.655, 2009.

667 Burnham, K. P. and Anderson, D. R.: Model Selection and Multi- Model Inference: A Practical
668 Information-Theoretic Approach, Springer, New York., 2002.

669 Chin, K. S., Lento, J., Culp, J. M., Lacelle, D., and Kokelj, S. V.: Permafrost thaw and intense thermokarst
670 activity decreases abundance of stream benthic macroinvertebrates, Glob. Chang. Biol., 22, 2715–
671 2728, doi:10.1111/gcb.13225, 2016.

672 Christ, M. J. and David, M. B.: Temperature and moisture effects on the production of dissolved organic
673 carbon in a Spodosol, Soil Biol. Biochem., 28, 1191–1199, doi:10.1016/0038-0717(96)00120-4, 1996.

674 Curtin, J.: lmSupport: Support for Linear Models. R package version 2.9.2., 2015.

675 Dittmar, T. and Kattner, G.: The biogeochemistry of the river and shelf ecosystem of the Arctic Ocean: a
676 review, Mar. Chem., 83, 103–120, doi:10.1016/S0304-4203(03)00105-1, 2003.

677 Drake, T. W., Wickland, K. P., Spencer, R. G. M., McKnight, D. M., and Striegl, R. G.: Ancient low–
678 molecular-weight organic acids in permafrost fuel rapid carbon dioxide production upon thaw, Proc.
679 Natl. Acad. Sci., 112, 13946–13951, doi:10.1073/pnas.1511705112, 2015.

680 Duk-Rodkin, A. and Hughes, O. L.: Surficial Geology, Fort McPherson-Bell River. Yukon-Northwest
681 Territories. Geological Survey of Canada, Map 1745A, scale 1:250 000, Geological Survey of Canada,
682 Map 1745A, scale 1:250 000, 1992.

683 Durbin, J. and Watson, G. S.: Testing for serial correlation in least squares regression I, Biometrika, 37,
684 409–428, 1950.

Environment Canada: Canadian Climate Normals 1981-2010 Station Data, Fort McPherson, 2015.

Fox, J. and Weisberg, S.: An {R} Companion to Applied Regression, Second Edition. Thousand Oaks CA: Sage. http://socserv.socsci.mcmaster.ca/jfox/Books/Companion., 2011.

Frey, K. E. and McClelland, J. W.: Impacts of permafrost degradation on arctic river biogeochemistry, Hydrol. Process., 23, 169–182, doi:10.1002/hyp, 2009.

Fritz, M., Vonk, J. E., and Lantuit, H.: Disappearing Arctic coastlines, Nat. Clim. Change, 7, 6-7, doi:10.1038/nclimate3188, 2017.

Fritz, M., Opel, T., Tanski, G., Herzschuh, U., Meyer, H., Eulenburg, A., and Lantuit, H.: Dissolved organic carbon (DOC) in Arctic ground ice, The Cryosphere, 9, 737-752, doi:10.5194/tc-9-737-2015, 2015.

Fritz, M., Wetterich, S., Schirrmeister, L., Meyer, H., Lantuit, H., Preusser, F., and Pollard, W. H.: Eastern Beringia and beyond: Late Wisconsinan and Holocene landscape dynamics along the Yukon Coastal Plain, Canada. Palaeogeogr. Palaeoclimatol. Palaeoecol., 319–320, 28–45, doi: 10.1016/j.palaeo.2011.12.015, 2012.

Fulton, R. J.: Surficial Materials of Canada, Natural Resources Canada., 1995.

Green, S. A. and Blough, N. V.: Optical absorption and fluorescence properties of chromophoric dissolved organic matter in natural waters, Limnol. Oceanogr., 39, 1903–1916, doi:10.4319/lo.1994.39.8.1903, 1994.

Hair, J. F. J., Anderson, R. E., Tatham, R. L., and Black, W. C.: Multivariate Data Analysis, 3rd ed., Macmillan, New York., 1995.

Hedges, J. I., Keil, R. G., and Benner, R.: What happens to terrestrial organic matter in the ocean?, Org. Geochem., 27, 195–212, 1997.

Helms, J. R., Stubbins, A., Ritchie, J. D., Minor, E. C., Kieber, D. J., and Mopper, K.: Absorption spectral slopes and slope ratios as indicators of molecular weight, source, and photobleaching of chromophoric dissolved organic matter, Limnol. Oceanogr., 53, 955–969, doi:10.4319/lo.2008.53.3.0955, 2008.

Holmes, R. M., McClelland, J. W., Peterson, B. J., Tank, S. E., Bulygina, E., Eglinton, T. I., Gordeev, V. V., Gurtovaya, T. Y., Raymond, P. A., Repeta, D. J., Staples, R., Striegl, R. G., Zhulidov, A. V., and Zimov, S. A.: Seasonal and annual fluxes of nutrients and organic matter from large rivers to the Arctic Ocean and surrounding seas, Estuaries and Coasts, 35, 369–382, doi:10.1007/s12237-011-9386-6, 2012.

Hugelius, G., Strauss, J., Zubrzycki, S., Harden, J. W., Schuur, E. A. G., Ping, C. L., Schirrmeister, L., Grosse, G., Michaelson, G. J., Koven, C. D., O'Donnell, J. A., Elberling, B., Mishra, U., Camill, P., Yu, Z., Palmtag, J., and Kuhry, P.: Estimated stocks of circumpolar permafrost carbon with quantified uncertainty ranges and identified data gaps, Biogeosciences, 11, 6573–6593, doi:10.5194/bg-11-6573-2014, 2014.

IPCC: Topic 2: Future Climate Changes, Risks, and Impacts In Climate Change 2014: Synthesis Report. Contribution of Working Groups I, II and III to the Fifth Assessment Report of the Intergovernmental Panel on Climate Change [Core Writing Team, R.K. Pachauri and L.A. Meyer (eds.)]. IPCC, Geneva,

722 Switzerland, 151 pp, Geneva, Switzerland., 2014.

723 Kaiser, K. and Guggenberger, G.: The role of DOM sorption to mineral surfaces in the preservation of
724 organic matter in soils, Org. Geochem., 31, 711–725, doi:10.1016/S0146-6380(00)00046-2, 2000.

725 Khvorostyanov, D. V., Krinner, G., Ciais, P., Heimann, M., and Zimov, S. A.: Vulnerability of permafrost
726 carbon to global warming. Part I: Model description and role of heat generated by organic matter
727 decomposition, Tellus, Ser. B Chem. Phys. Meteorol., 60 B, 250–264, doi:10.1111/j.1600-
728 0889.2007.00333.x, 2008a.

729 Khvorostyanov, D. V., Ciais, P., Krinner, G., Zimov, S. A., Corradi, C., and Guggenberger, G.: Vulnerability
730 of permafrost carbon to global warming. Part II: Sensitivity of permafrost carbon stock to global
731 warming, Tellus, Ser. B Chem. Phys. Meteorol., 60 B, 265–275, doi:10.1111/j.1600-
732 0889.2007.00336.x, 2008b.

733 Kokelj, S. V, Tunnicliffe, J. F., and Lacelle, D.: The Peel Plateau of northwestern Canada : an ice-rich
734 hummocky moraine landscape in transition, in Landscapes and Landforms of western Canada,
735 edited by O. Slaymaker, pp. 109–122, Springer International Publishing, Switzerland., 2017a.

736 Kokelj, S. V. and Jorgenson, M. T.: Advances in thermokarst research, Permafr. Periglac. Process., 24,
737 108–119, doi:10.1002/ppp.1779, 2013.

738 Kokelj, S. V., Smith, C. A., and Burn, C. R.: Physical and chemical characteristics of the active layer and
739 permafrost, Herschel Island, western Arctic Coast, Canada, Permafr. Periglac. Process., 13, 171–185,
740 doi:10.1002/ppp.417, 2002.

741 Kokelj, S. V., Jenkins, R. E., Milburn, D., Burn, C. R., and Snow, N.: The influence of thermokarst
742 disturbance on the water quality of small upland lakes, Mackenzie Delta region, Northwest
743 Territories, Canada, Permafr. Periglac. Process., 16, 343–353, doi:10.1002/ppp.536, 2005.

744 Kokelj, S. V., Lantz, T. C., Kanigan, J. C., Smith, S. L., and Coutts, R.: Origin and polycyclic behaviour of
745 tundra thaw slumps, Mackenzie Delta region, Northwest Territories, Canada, Permafr. Periglac.
746 Process., 20, 173–184, doi:10.1002/ppp, 2009.

747 Kokelj, S. V., Lacelle, D., Lantz, T. C., Tunnicliffe, J., Malone, L., Clark, I. D., and Chin, K. S.: Thawing of
748 massive ground ice in mega slumps drives increases in stream sediment and solute flux across a
749 range of watershed scales, J. Geophys. Res. Earth Surf., 118, 681–692, doi:10.1002/jgrf.20063, 2013.

750 Kokelj, S. V., Tunnicliffe, J., Lacelle, D., Lantz, T. C., Chin, K. S., and Fraser, R.: Increased precipitation
751 drives mega slump development and destabilization of ice-rich permafrost terrain, northwestern
752 Canada, Glob. Planet. Change, 129, 56–68, doi:10.1016/j.gloplacha.2015.02.008, 2015.

753 Kokelj, S. V., Lantz, T. C., Tunnicliffe, J., Segal, R., and Lacelle, D.: Climate-driven thaw of permafrost
754 preserved glacial landscapes, northwestern Canada, Geology, 45, 371–374, doi:10.1130/G38626.1,
755 2017b.

756 Kothawala, D. N., Moore, T. R., and Hendershot, W. H.: Soil properties controlling the adsorption of
757 dissolved organic carbon to mineral soils, Soil Sci. Soc. Am. J., 73, 1831–1842,
758 doi:10.2136/sssaj2008.0254, 2009.

759 Lacelle, D., Bjornson, J., and Lauriol, B.: Climatic and geomorphic factors affecting contemporary (1950-
760 2004) activity of retrogressive thaw slumps on the Aklavik Plateau, Richardson Mountains, NWT,
761 Canada, Permafr. Periglac. Process., 21, 1–15, doi:10.1002/ppp.666, 2010.

762 Lacelle, D., Lauriol, B., Zazula, G., Ghaleb, B., Utting, N., and Clark, I. D.: Timing of advance and basal
763 condition of the Laurentide Ice Sheet during the last glacial maximum in the Richardson Mountains,
764 NWT, Quat. Res. (United States), 80, 274–283, doi:10.1016/j.yqres.2013.06.001, 2013.

765 Lacelle, D., Fontaine, M., Forest, A. P., and Kokelj, S.: High-resolution stable water isotopes as tracers of
766 thaw unconformities in permafrost: A case study from western Arctic Canada, Chem. Geol., 368, 85–
767 96, doi:10.1016/j.chemgeo.2014.01.005, 2014.

768 Lacelle, D., Brooker, A., Fraser, R. H., and Kokelj, S. V.: Distribution and growth of thaw slumps in the
769 Richardson Mountains–Peel Plateau region, northwestern Canada, Geomorphology, 235, 40–51,
770 doi:10.1016/j.geomorph.2015.01.024, 2015.

771 Lafrenière, M. J. and Lamoureux, S. F.: Thermal perturbation and rainfall runoff have greater impact on
772 seasonal solute loads than physical disturbance of the active layer, Permafr. Periglac. Process., 24,
773 241–251, doi:10.1002/ppp.1784, 2013.

774 Lang, S. Q., McIntyre, C. P., Bernasconi, S. M., Früh-Green, G. L., Voss, B. M., Eglinton, T. I., and Wacker,
775 L.: Rapid 14C analysis of dissolved organic carbon in non-saline waters, Radiocarbon, 58, 505–515,
776 doi:10.1017/RDC.2016.17, 2016.

777 Lantuit, H. and Pollard, W. H.: Fifty years of coastal erosion and retrogressive thaw slump activity on
778 Herschel Island, southern Beaufort Sea, Yukon Territory, Canada, Geomorphology, 95, 84–102,
779 doi:10.1016/j.geomorph.2006.07.040, 2008.

780 Lantuit, H., Pollard, W. H., Couture, N., Fritz, M., Schirrmeister, L., Meyer, H., and Hubberten, H.W.:
781 Modern and late Holocene retrogressive thaw slump activity on the Yukon Coastal Plain and
782 Herschel Island, Yukon Territory, Canada. Permafrost Periglacial Process. 23, 39–51, doi:
783 10.1002/ppp.1731, 2012.

784 Lantz, T. C. and Kokelj, S. V.: Increasing rates of retrogressive thaw slump activity in the Mackenzie Delta
785 region, N.W.T., Canada, Geophys. Res. Lett., 35, 1–5, doi:10.1029/2007GL032433, 2008.

786 Lewkowicz, A. G.: Rate of short-term ablation of exposed ground ice, Banks Island, Northwest
787 Territories, Canada, J. Glaciol., 32, 511–519, 1986.

788 Lewkowicz, A. G.: Headwall retreat of ground-ice slumps, Banks Island, Northwest Territories, Can. J.
789 Earth Sci., 24, 1077–1085, doi:10.1139/e87-105, 1987.

790 MacLean, R., Oswood, M. W., Irons, J. G., and McDowell, W. H.: The effect of permafrost on stream
791 biogeochemistry: A case study of two streams in the Alaskan (U.S.A.) taiga, Biogeochemistry, 47,
792 239–267, doi:10.1007/BF00992909, 1999.

793 Malone, L., Lacelle, D., Kokelj, S., and Clark, I. D.: Impacts of hillslope thaw slumps on the geochemistry
794 of permafrost catchments (Stony Creek watershed, NWT, Canada), Chem. Geol., 356, 38–49,
795 doi:10.1016/j.chemgeo.2013.07.010, 2013.

796 Manley, W. F. and Kaufman, D. S.: Alaska PaleoGlacier Atlas: Institute of Arctic and Alpine Research
797 (INSTAAR), University of Colorado., 2002.

798 Mann, P. J., Davydova, A., Zimov, N., Spencer, R. G. M., Davydov, S., Bulygina, E., Zimov, S., and Holmes,
799 R. M.: Controls on the composition and lability of dissolved organic matter in Siberia's Kolyma River
800 basin, J. Geophys. Res. Biogeosciences, 117, G01028, doi:10.1029/2011JG001798, 2012.

801 Mann, P. J., Eglinton, T. I., McIntyre, C. P., Zimov, N., Davydova, A., Vonk, J. E., Holmes, R. M., and
802 Spencer, R. G. M.: Utilization of ancient permafrost carbon in headwaters of Arctic fluvial networks,
803 Nat. Commun., 6, 7856, doi: 10.1038/ncomms8856, 2015.

804 McDowell, W. H.: Kinetics and mechanisms of dissolved organic carbon retention in a headwater stream,
805 Biogeochemistry, 1, 329–352, 1985.

806 Murton, J. and French, H.: Cryostructures in permafrost, Tuktoyaktuk coastlands, western arctic Canada,
807 Can. J. Earth Sci., 31, 737–747, doi:10.1139/e94-067, 1994.

808 Murton, J. B., Edwards, M. E., Lozhkin, A. V, Anderson, P. M., Savvinov, G. N., Bakulina, N., Bondarenko,
809 O. V, Cherepanova, M. V, Danilov, P. P., Boeskorov, V., Goslar, T., Grigoriev, S., Gubin, S. V, Korzun, J.
810 A., Lupachev, A. V, Tikhonov, A., Tsygankova, V. I., Vasilieva, G. V., and Zanina, O. G.: Preliminary
811 paleoenvironmental analysis of permafrost deposits at Batagaika megaslump, Yana Uplands,
812 northeast Siberia, Quat. Res., 87, 314–330, doi:10.1017/qua.2016.15, 2017.

813 Neff, J. C. and Hooper, D. U.: Vegetation and climate controls on potential CO2, DOC and DON
814 production in northern latitude soils, Glob. Chang. Biol., 8, 872–884, doi:10.1046/j.1365-
815 2486.2002.00517.x, 2002.

816 Neff, J. C., Finlay, J. C., Zimov, S. A., Davydov, S. P., Carrasco, J. J., Schuur, E. A. G., and Davydova, A. I.:
817 Seasonal changes in the age and structure of dissolved organic carbon in Siberian rivers and streams,
818 Geophys. Res. Lett., 33, 1–5, doi:10.1029/2006GL028222, 2006.

819 Norris, D. K.: Geology of the northern Yukon and northwestern District of Mackenzie. Geological Survey
820 of Canada, Map 1581A, scale 1:500 000, 1984.

821 O'Donnell, J. A., Aiken, G. R., Kane, E. S., and Jones, J. B.: Source water controls on the character and
822 origin of dissolved organic matter in streams of the Yukon River basin, Alaska, J. Geophys. Res.
823 Biogeosciences, 115, 1–12, doi:10.1029/2009JG001153, 2010.

824 Olefeldt, D., Goswami, S., Grosse, G., Hayes, D., Hugelius, G., Kuhry, P., McGuire, A. D., Romanovsky, V.
825 E., Sannel, A. B. K., Schuur, E. A. G., and Turetsky, M. R.: Circumpolar distribution and carbon storage
826 of thermokarst landscapes, 7, 13043, 2016.

827 Palstra, S. and Meijer, H.: Biogenic carbon fraction of biogas and natural gas fuel mixtures determined
828 with 14C, Radiocarbon, 56, 7–28, doi:10.2458/56.16514, 2014.

829 Pinheiro, J., Bates, D., DebRoy, S., Sarkar, D., and R Core Team: nlme: Linear and nonlinear mixed effects
830 models. R package version 3.1-120, http://CRAN.R-project.org/package=nlme>., 2015.

831 Poulin, B. A., Ryan, J. N., and Aiken, G. R.: Effects of iron on optical properties of dissolved organic
832 matter, Environ. Sci. Technol., 48, 10098–10106, doi:10.1021/es502670r, 2014.

Prokushkin, A. S., Kajimoto, T., Prokushkin, S. G., McDowell, W. H., Abaimov, A. P., and Matsuura, Y.: Climatic factors influencing fluxes of dissolved organic carbon from the forest floor in a continuous-permafrost Siberian watershed, Can. J. For. Res., 35, 2130–2140, doi:10.1139/x05-150, 2005.

Pumpanen, J., A, L., Heli, M., Kolari, P., Ilvesniemi, H., Mammarella, I., Hari, O., Nikinmaa, E., Heinonsalo, J., Back, J., Ojala, A., Berninger, F., and Vesala, T.: Precipitation and net ecosystem exchange are the most important drivers of DOC flux in upland boreal catchments, J. Geophys. Res. Biogeosciences, 119, 1861–1878, doi:10.1002/2014JG002705, 2014.

Qualls, R. and Haines, B. L.: Measuring adsorption isotherms using continuous, unsaturated flow through intact soil cores, Soil Sci. Soc. Am. J., 56, 456–460, doi:10.2136/sssaj1992.03615995005600020019x, 1992.

R Core Team: R: A Language and Environment for Statistical Computing, R Foundation for Statistical Computing, Vienna, Austria. http://www.r-project.org/., 2015.

Rampton, V. N.: Quaternary geology of the Tuktoyaktuk coastlands, Northwest Territories, Geol. Surv. Canada, 1988.

Romanovsky, V. E., Smith, S. L., and Christiansen, H. H.: Permafrost thermal state in the polar Northern Hemisphere during the international polar year 2007–2009: a synthesis, Permafrost Periglacial Process., 21, 106-116, doi: 10.1002/ppp.689, 2010.

Schuur, E., Bockheim, J., Canadell, J. G., Euskirchen, E., Field, C. B., Goryachkin, S. V, Hagemann, S., Kuhry, P., Lafleur, P. M., Lee, H., Nelson, M. F. E., Rinke, A., Romanovsky, V. E., Shiklomanov, N., Tarnocai, C., Venevsky, S., Vogel, J. G., and Zimov, S. A.: Vulnerability of permafrost carbon to climate change : Implications for the global carbon cycle, Bioscience, 58, 701–714, doi:10.1641/B580807, 2008.

Schuur, E. A. G., Abbott, B. W., Bowden, W. B., Brovkin, V., Camill, P., Canadell, J. G., Chanton, J. P., Chapin, F. S., Christensen, T. R., Ciais, P., Crosby, B. T., Czimczik, C. I., Grosse, G., Harden, J., Hayes, D. J., Hugelius, G., Jastrow, J. D., Jones, J. B., Kleinen, T., Koven, C. D., Krinner, G., Kuhry, P., Lawrence, D. M., McGuire, A. D., Natali, S. M., O'Donnell, J. A., Ping, C. L., Riley, W. J., Rinke, A., Romanovsky, V. E., Sannel, A. B. K., Schädel, C., Schaefer, K., Sky, J., Subin, Z. M., Tarnocai, C., Turetsky, M. R., Waldrop, M. P., Walter Anthony, K. M., Wickland, K. P., Wilson, C. J., and Zimov, S. A.: Expert assessment of vulnerability of permafrost carbon to climate change, Clim. Change, 119, 359–374, doi:10.1007/s10584-013-0730-7, 2013.

Schuur, E. A. G., McGuire, A. D., Grosse, G., Harden, J. W., Hayes, D. J., Hugelius, G., Koven, C. D., and Kuhry, P.: Climate change and the permafrost carbon feedback, Nature, 520, 171–179, doi:10.1038/nature14338, 2015.

Segal, R. A., Lantz, T. C., and Kokelj, S. V: Acceleration of thaw slump activity in glaciated landscapes of the Western Canadian Arctic, Environ. Res. Lett., 11, 34025, doi:10.1088/1748-9326/11/3/034025, 2016.

Spencer, R. G. M., Mann, P. J., Dittmar, T., Eglinton, T. I., Mcintyre, C., Holmes, R. M., Zimov, N., and Stubbins, A.: Detecting the signature of permafrost thaw in Arctic rivers, Geophys. Res. Lett., 42, doi:10.1002/2015GL063498, doi:10.1002/2015GL063498, 2015.

872 Street, L. E., Dean, J. F., Billett, M. F., Baxter, R., Dinsmore, K. J., Lessels, J. S., Subke, J.-A., Tetzlaff, D.,
873 and Wookey, P. A.: Redox dynamics in the active layer of an Arctic headwater catchment; examining
874 the potential for transfer of dissolved methane from soils to stream water, J. Geophys. Res.
875 Biogeosci., 121, 2776-2792, doi: 10.1002/2016JG003387, 2016.

876 Striegl, R. G., Aiken, G. R., Dornblaser, M. M., Raymond, P. A., and Wickland, K. P.: A decrease in
877 discharge-normalized DOC export by the Yukon River during summer through autumn, Geophys.
878 Res. Lett., 32, 1–4, doi:10.1029/2005GL024413, 2005.

879 Tank, S. E., Raymond, P. A., Striegl, R. G., McClelland, J. W., Holmes, R. M., Fiske, G. J., and Peterson, B.
880 J.: A land-to-ocean perspective on the magnitude, source and implication of DIC flux from major
881 Arctic rivers to the Arctic Ocean, Global Biogeochem. Cycles, 26, GB4018,
882 doi:10.1029/2011GB004192, 2012a.

883 Tank, S. E., Manizza, M., Holmes, R. M., McClelland, J. W., and Peterson, B. J.: The processing and impact
884 of dissolved riverine nitrogen in the Arctic Ocean, Estuaries and Coasts, 35, 401–415,
885 doi:10.1007/s12237-011-9417-3, 2012b.

886 Tanski, G., Couture, N., Lantuit, H., Eulenburg, A., and Fritz, M.: Eroding permafrost coasts release low
887 amounts of dissolved organic carbon (DOC) from ground ice into the nearshore zone of the Arctic
888 Ocean, Glob. Biogeochem. Cycles, 30, 1054–1068, doi:10.1002/2015GB005337, 2016.

889 Tanski, G., Lantuit, H., Ruttor, S., Knoblauch, C., Radosavljevic, B., Strauss, J., Wolter, J., Irrgang, A. M.,
890 Ramage, J., and Fritz, M.: Transformation of terrestrial organic matter along thermokarst-affected
891 permafrost coasts in the Arctic. Sci. Total Environ. 581–582, 434-447, doi:
892 10.1016/j.scitotenv.2016.12.152, 2017.

893 Thompson, M. S., Prowse, T. D., Kokelj, S. V., and Wrona, F. J.: The impact of sediments derived from
894 thawing permafrost on tundra lake water chemistry: An experimental approach, Proc. Ninth Int.
895 Conf. Permafr., 29, 1763–1768, 2008.

896 Vonk, J. E. and Gustafsson, Ö.: Permafrost-carbon complexities, Nat. Geosci., 6, 675–676,
897 doi:10.1038/ngeo1937, 2013.

898 Vonk, J. E., Mann, P. J., Dowdy, K. L., Davydova, A., Davydov, S. P., Zimov, N., Spencer, R. G. M., Bulygina,
899 E. B., Eglinton, T. I., and Holmes, R. M.: Dissolved organic carbon loss from Yedoma permafrost
900 amplified by ice wedge thaw, Environ. Res. Lett., 8, 35023, doi:10.1088/1748-9326/8/3/035023,
901 2013a.

902 Vonk, J. E., Mann, P. J., Davydov, S., Davydova, A., Spencer, R. G. M., Schade, J., Sobczak, W. V., Zimov,
903 N., Zimov, S., Bulygina, E., Eglinton, T. I., and Holmes, R. M.: High biolability of ancient permafrost
904 carbon upon thaw, Geophys. Res. Lett., 40, 2689–2693, doi:10.1002/grl.50348, 2013b.

905 Vonk, J. E., Tank, S. E., Mann, P. J., Spencer, R. G. M., Treat, C. C., Striegl, R. G., Abbott, B. W., and
906 Wickland, K. P.: Biodegradability of dissolved organic carbon in permafrost soils and waterways: a
907 meta-analysis, Biogeosciences, 12, 6915–6930, doi:10.5194/bgd-12-8353-2015, 2015a.

908 Vonk, J. E., Tank, S. E., Bowden, W. B., Laurion, I., Vincent, W. F., Alekseychik, P., Amyot, M., Billet, M. F.,
909 Canário, J., Cory, R. M., Deshpande, B. N., Helbig, M., Jammet, M., Karlsson, J., Larouche, J.,
910 Macmillan, G., Rautio, M., Walter Anthony, K. M., and Wickland, K. P.: Reviews and syntheses:

911 Effects of permafrost thaw on Arctic aquatic ecosystems, Biogeosciences, 12, 7129–7167,
912 doi:10.5194/bg-12-7129-2015, 2015b.

913 Ward, R. C. and Robinson, M.: Principles of Hydrology, Fourth Edition, McGraw-Hill International (UK)
914 Limited., 2000.

915 Watanabe, S., Laurion, I., Chokmani, K., Pienitz, R., and Vincent, W. F.: Optical diversity of thaw ponds in
916 discontinuous permafrost: A model system for water color analysis, J. Geophys. Res. Biogeosciences,
917 116, doi:10.1029/2010JG001380, 2011.

918 Weishaar, J. and Aiken, G.: Evaluation of specific ultra-violet absorbance as an indicator of the chemical
919 content of dissolved organic carbon, Environ. Chem., 37, 4702–4708, doi:10.1021/es030360x, 2003.

920 Woods, G. C., Simpson, M. J., Pautler, B. G., Lamoureux, S. F., Lafrenière, M. J., and Simpson, A. J.:
921 Evidence for the enhanced lability of dissolved organic matter following permafrost slope
922 disturbance in the Canadian High Arctic, Geochim. Cosmochim. Acta, 75, 7226–7241,
923 doi:10.1016/j.gca.2011.08.013, 2011.

924 Yanagihara, Y., Koike, T., Matsuura, Y., Mori, S., Shibata, H., Satoh, F., Masuyagina, O., Zyryanova, O.,
925 Prokushkin, A. S., Prokushkin, S. G., and Abaimov, A. P.: Soil respiration on the contrasting north-
926 and south-facing slopes of a larch forests in Central Siberia, Eurasian J. For. Res., 1, 19–29, 2000.

927 Zeileis, A. and Grothendieck, G.: zoo: S3 infrastructure for regular and irregular time series, J. Stat.
928 Softw., 14, 1–27, 2005.

929 Zeileis, A. and Hothorn, T.: Diagnostic checking in regression relationships., R News, 2, 7–10, 2002.

930 Zhou, Y., Guo, H., Lu, H., Mao, R., Zheng, H., and Wang, J.: Analytical methods and application of stable
931 isotopes in dissolved organic carbon and inorganic carbon in groundwater, Rapid Commun. Mass
932 Spectrom., 29, 1827–1835, doi:10.1002/rcm.7280, 2015.

933 Zuur, A. F., Ieno, E. N., Walker, N., Saveliev, A. A., and Smith, G. M.: Mixed Effects Models and Extensions
934 in Ecology with R, Springer, New York., 2009.

935

936

Table 1: Slump characteristics and sampling information for eight retrogressive thaw slumps sampled during the 2014 field season on the Peel Plateau, NWT, Canada. Characteristics are derived from published values and field estimations.

Slump location	Sample dates (Julian day)[a]	Latitude	Longitude	Area (ha)	Debris tongue (m)[b]	Headwall height (m)
FM4	202, 210, 223	67 16.679	-135 09.573	8.8	960	16 to 20[d]
FM2	200, 209, 222	67 15.462	-135 14.216	31.7	1529	25[e]
FM3	197, 212	67 15.100	-135 16.270	6.1	576	10[e]
SD	196, 213, 234	67 10.818	-135 43.630	3.3	NA	2 – 4[d]
HA	190, 229	67 09.057	-135 41.121	5.9	288	6 – 10[d]
HB	190, 229	67 14.397	-135 49.167	13.6[c]	257	6 – 10[d]
HC	190, 229	67 19.652	-135 53.620	10.3, 10.3[c]	408	6 – 10[d]
HD	190, 229	67 24.025	-135 20.048	1.8	137	6 – 10[d]
Weather Station		67 14.756	-135 12.920			

[a] Excludes samples for the FM3 'environmental controls' analysis which was conducted on 17 additional dates; HD, Julian date 229 did not include a within-slump sample.

[b] The length of debris tongue measured from the base of the debris scar, along the valley bottom stream

[c] Site HB is comprised of two smaller slump features that have merged into the scar zone delineated here; site HC is comprised of 5 separate slump features that have merged into two scar zones, each with an area of 10.3 ha

[d] Rough estimates by field crews over 2014 and 2015 field seasons

[e] Kokelj et al. 2015

Table 2: Results of the mixed-effects models used to assess the effects of slumping on stream water chemistry and optical characteristics. Downstream models incorporated data from downstream and upstream sites; within-slump models incorporated data from within-slump and upstream sites. Provided are degrees of freedom (df), t-statistics, and p-values for individual model runs. Further details on the statistical approach are provided in Section 3.4.

	Downstream			Within-slump		
	df	**t**	**p**	**df**	**t**	**p**
DOC	20	-12.895	<.0001	30	-1.468	0.153
Na	33	9.662	<.0001	30	7.278	0.000
Ca	33	9.767	<.0001	30	4.782	0.000
Mg	33	6.166	<.0001	30	8.593	0.000
Conductivity	32	43.083	<.0001	30	11.895	0.000
TSS	29	6.692	<.0001	28	2.187	0.037
SUVA	32	-4.460	<.0001	30	-35.052	0.000
S_R	32	5.333	<.0001	31	8.065	0.000
S_{275}	31	2.856	0.008	31	8.159	0.000
S_{350}	32	-2.196	0.036	31	16.665	0.000

960 **Table 3:** Measured fraction modern carbon ($F^{14}C$) and estimated calendar years before present for ^{14}C of
961 dissolved organic carbon samples collected upstream of, and within drainage waters of, selected slump
962 sites. Data were collected during the summer of 2016. nc indicates sample not collected. Error
963 estimates indicate 1σ.

964

	$F^{14}C$		^{14}C yr BP	
Site	Upstream	Within-slump	Upstream	Within-slump
FM4	0.9734 ± 0.0029	nc	217 ± 24	nc
FM2	0.9764 ± 0.0032	0.3030 ± 0.0024	192 ± 27	9592 ± 64
FM3	1.0023 ± 0.0030	0.3618 ± 0.0018	modern	8167 ± 39
SD	1.0216 ± 0.0035	0.8659 ± 0.0025	modern	1157 ± 23

965

966

967 **Table 4:** Results of multiple linear regression analyses to assess environmental controls on upstream and downstream DOC flux, and upstream
968 and downstream DOC concentration. nr indicates variables that were not retained in the best fit regression model; NA indicates variables that
969 were not run in individual analyses. Significant p-values are indicated with bold text; marginal results (0.05 < p < 0.10) are indicated in italics.
970 Model statistics are as follows: downstream flux r^2=0.84, $F_{7,11}$=8.25, p = 0.001; upstream flux r^2=0.87, $F_{7,11}$=10.79, p <0.001; downstream
971 concentration r^2=0.85, $F_{4,14}$=19.57, p < 0.001; upstream concentration r^2=0.91, $F_{5,13}$=27.05, p < 0.001.

	Downstream DOC flux			Upstream DOC flux			Downstream DOC concentration			Upstream DOC concentration		
Coefficient	Estimate	t	p	Estimate	t	p	Estimate	t	p	Estimate	t	p
Average Air Temperature (^oC)												
0 h	-67.08	-1.685	0.120	**-115.96**	**-3.286**	**0.007**	nr	nr	nr	**0.165**	**2.349**	**0.035**
48 h	nr	nr	nr	56.32	1.534	0.153	**0.332**	**6.886**	**<0.001**	**0.396**	**5.510**	**<0.001**
72 h	**-95.15**	**-2.594**	**0.025**	**-94.17**	**-2.717**	**0.020**	nr	nr	nr	nr	nr	nr
120 h	nr	nr	nr	nr	nr	nr	**0.134**	**3.527**	**0.003**	**0.203**	**4.411**	**<0.001**
Rainfall (mm)												
0h	**116.13**	**5.411**	**<0.001**	**105.47**	**6.039**	**<0.001**	*-0.066*	*-1.967*	*0.069*	nr	nr	nr
48h	nr	nr	nr	nr	nr	nr	nr	nr	nr	nr	nr	nr
72h	nr	nr	nr	nr	nr	nr	nr	nr	nr	nr	nr	nr
120h	*-23.94*	*-1.970*	*0.075*	**-24.15**	**-2.529**	**0.028**	nr	nr	nr	nr	nr	nr
Average net radiation (W m^{-2})												
0h	4.96	1.286	0.225	nr	nr	nr	**-0.021**	**-4.043**	**0.001**	**-0.021**	**-3.387**	**0.005**
48h	nr	nr	nr	nr	nr	nr	nr	nr	nr	nr	nr	nr
72h	5.58	1.545	0.151	4.04	1.563	0.146	nr	nr	nr	nr	nr	nr
120h	nr	nr	nr	nr	nr	nr	nr	nr	nr	nr	nr	nr
Total suspended solids (mg L^{-1})												
Downstream	*-0.02*	*-2.102*	*0.059*	NA	NA	NA	nr	nr	nr	NA	NA	NA
Upstream	NA	NA	NA	-0.32	-1.626	0.132	NA	NA	NA	-0.0006	-1.627	0.128

972

Figure captions:

Fig. 1*:* Location and morphology of thaw slumps on the Peel Plateau, Northwest Territories, Canada. Panel A depicts the stream networks and location of the eight retrogressive thaw slumps studied. Panel B depicts representative sampling locations at each slump site; FM3 depicted. Panels C-E depict representative thaw-slump headwall stratigraphies. Panel C shows a mega-slump (FM3, the smallest mega-slump, is depicted); panel D shows a moderate-sized slump (HB); panel E shows the smallest slump that was sampled (SD). In panels C and D, the approximate location of the modern active layer (a), early Holocene-aged relict active layer (b), and Pleistocene-aged glacigenic materials (c) is shown. Photo credit: Scott Zolkos.

Fig. 2: The effect of retrogressive thaw slumps on stream water dissolved organic carbon (DOC) concentration. Each data point represents the mean and standard error of measurements across all sampling dates, as described in Table 1. The bottom two panels show the ratio of within-slump: upstream, and downstream: upstream DOC concentrations within individual slumps, with points indicating the mean and standard error of this ratio across sample dates.

Fig. 3: Box and whisker plots to illustrate the effects of retrogressive thaw slump activity on stream geochemistry. Each boxplot includes data from across all slumps and sampling periods, and indicates median values, 25^{th} and 75^{th} percentiles (box extremities), 10^{th} and 90^{th} percentiles (whiskers), and outlier points. U=upstream sites; W=within-slump sites; D=downstream sites.

Fig. 4: The effect of retrogressive thaw slumps on the optical properties of stream water dissolved organic matter. Each data point represents the mean and standard error of measurements across all sampling dates, as described in Table 1. Shown are specific UV absorbance ($SUVA_{254}$), spectral slopes between 275-295 and 350-400 nm ($S_{275-295}$; $S_{350-400}$) and the slope ratio (S_R).

Fig. 5: Paired oxygen isotopic ($\delta^{18}O$ ‰) and $SUVA_{254}$ (L mg $C^{-1}m^{-1}$) data, to demonstrate the relationship between source water age and dissolved organic matter composition. Reference $\delta^{18}O$ values are from Lacelle et al. (2013): the modern active layer value is derived from active layer pore water in this region, icy diamicton has been souced as Holocene in origin, and the $\delta^{18}O$ value for Pleistocene-aged ground ice is the most positive value for this region.

Fig. 6: Environmental conditions (solar radiation, precipitation and mean daily air temperature) and DOC flux upstream and downstream of slump FM3 across a month-long sample period (July 12-August 12, 2014). Corresponding multiple linear regressions are described in Table 4.

Fig. 7: Within-slump fluxes of dissolved organic carbon (DOC), and TSS, compared to the calculated (downstream - upstream) fluxes for these two constituents. TSS – a conservative tracer over short distances – shows an additive response where the measured within-slump flux is equivalent to the calculated (downstream - upstream) flux. In contrast, DOC shows clear evidence of downstream loss.

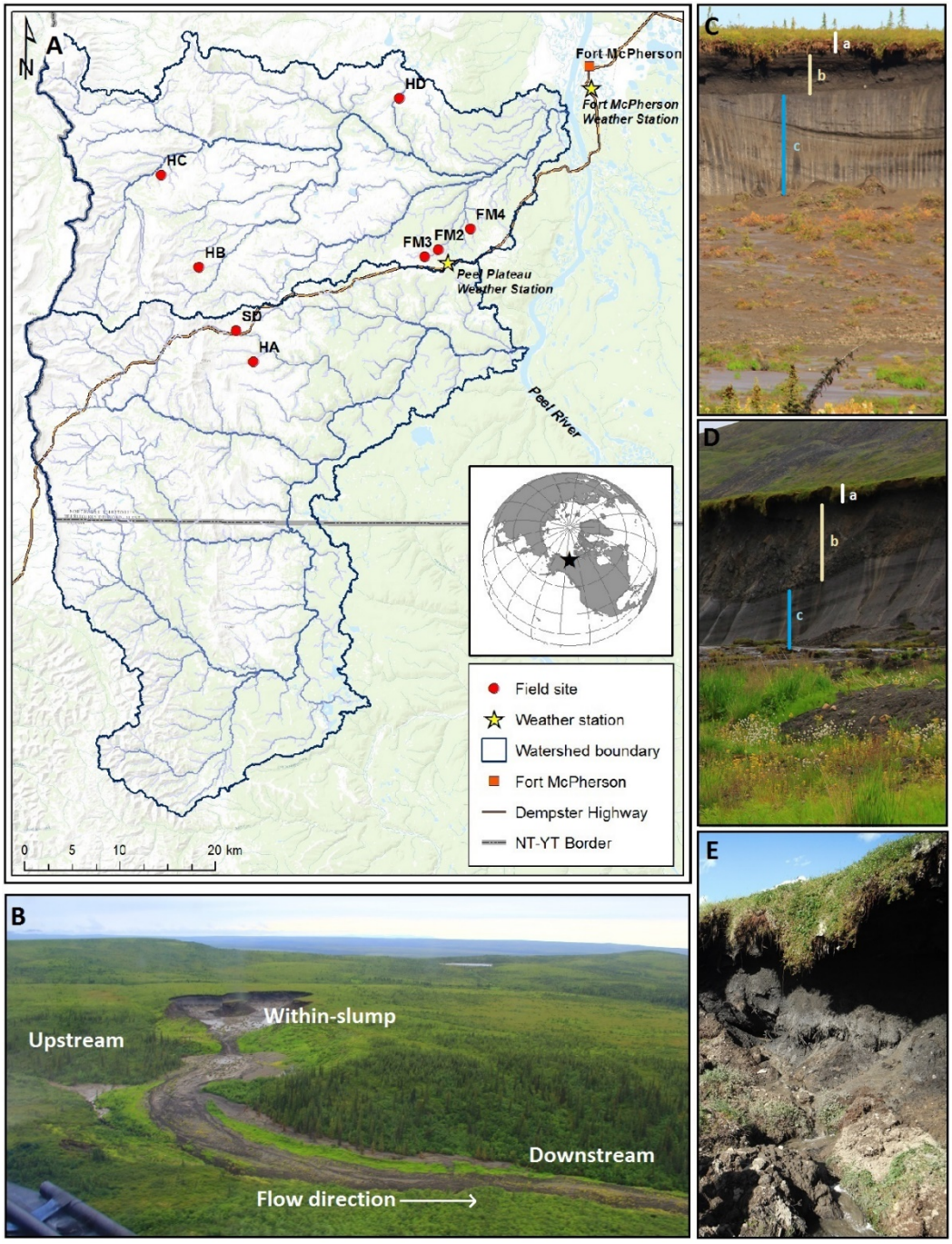

Fig. 1*:* Location and morphology of thaw slumps on the Peel Plateau, Northwest Territories, Canada. Panel A depicts the stream networks and location of the eight retrogressive thaw slumps studied. Panel B depicts representative sampling locations at each slump site; FM3 depicted. Panels C-E depict representative thaw-slump headwall stratigraphies. Panel C shows a mega-slump (FM3, the smallest mega-slump, is depicted); panel D shows a moderate-sized slump (HB); panel E shows the smallest slump that was sampled (SD). In panels C and D, the approximate location of the modern active layer (a), early Holocene-aged relict active layer (b), and Pleistocene-aged glacigenic materials (c) is shown. Photo credit: Scott Zolkos.

1017

1018

1019

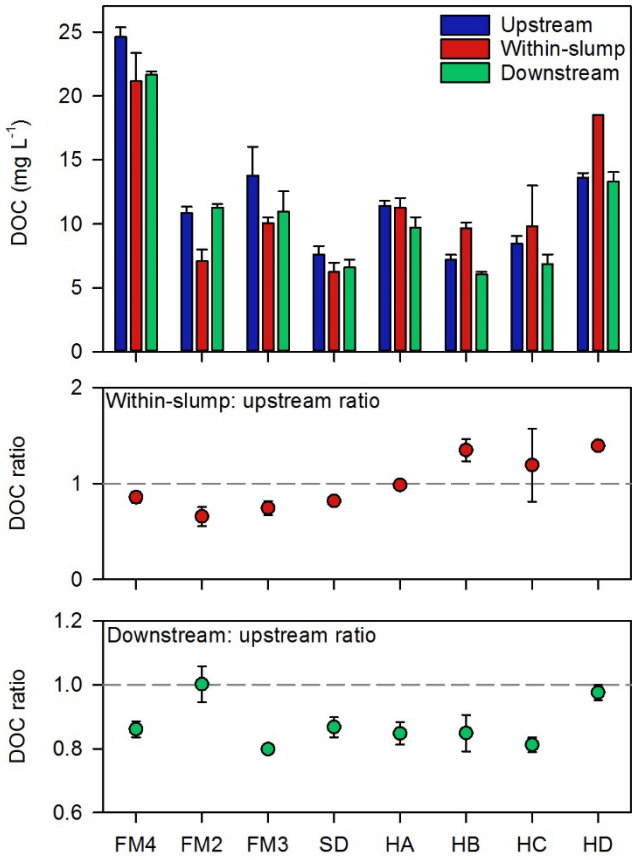

1020 **Fig. 2:** The effect of retrogressive thaw slumps on stream water dissolved organic carbon (DOC)
1021 concentration. Each data point represents the mean and standard error of measurements across all
1022 sampling dates, as described in Table 1. The bottom two panels show the ratio of within-slump:
1023 upstream, and downstream: upstream DOC concentrations within individual slumps, with points
1024 indicating the mean and standard error of this ratio across sample dates.

1025

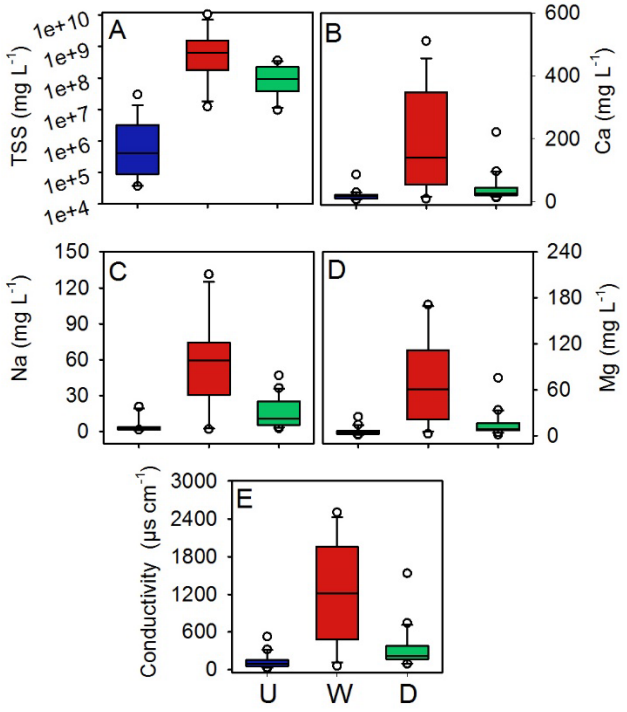

1026

1027 **Fig. 3:** Box and whisker plots to illustrate the effects of retrogressive thaw slump activity on stream
1028 geochemistry. Each boxplot includes data from across all slumps and sampling periods, and indicates
1029 median values, 25th and 75th percentiles (box extremities), 10th and 90th percentiles (whiskers), and
1030 outlier points. U=upstream sites; W=within-slump sites; D=downstream sites.

1031

1032

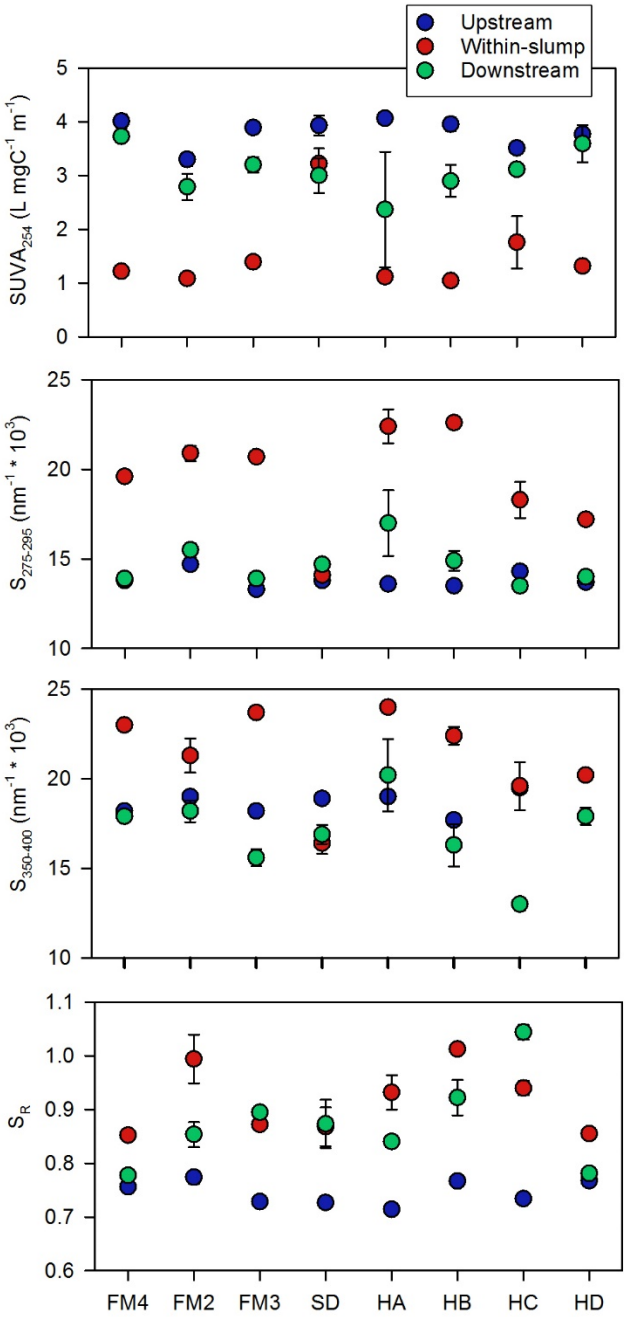

1033 **Fig. 4:** The effect of retrogressive thaw slumps on the optical properties of stream water dissolved
1034 organic matter. Each data point represents the mean and standard error of measurements across all
1035 sampling dates, as described in Table 1. Shown are specific UV absorbance ($SUVA_{254}$), spectral slopes
1036 between 275-295 and 350-400 nm ($S_{275-295}$; $S_{350-400}$) and the slope ratio (S_R).

1037

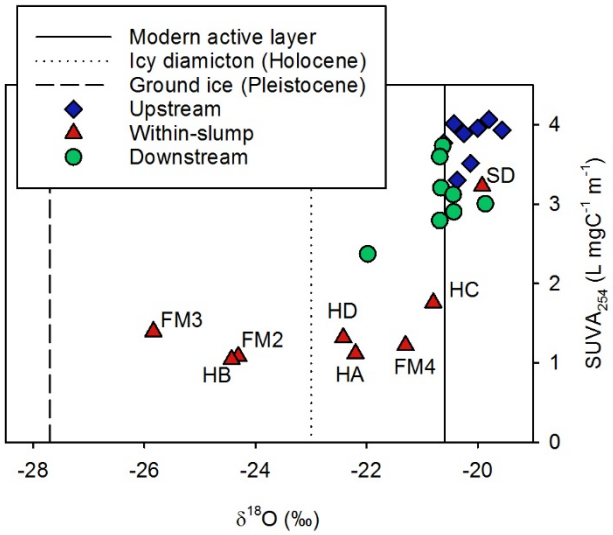

Fig. 5: Paired oxygen isotopic ($\delta^{18}O$ ‰) and $SUVA_{254}$ (L mg $C^{-1}m^{-1}$) data, to demonstrate the relationship between source water age and dissolved organic matter composition. Reference $\delta^{18}O$ values are from Lacelle et al. (2013): the modern active layer value is derived from active layer pore water in this region, icy diamicton has been souced as Holocene in origin, and the $\delta^{18}O$ value for Pleistocene-aged ground ice is the most positive value for this region.

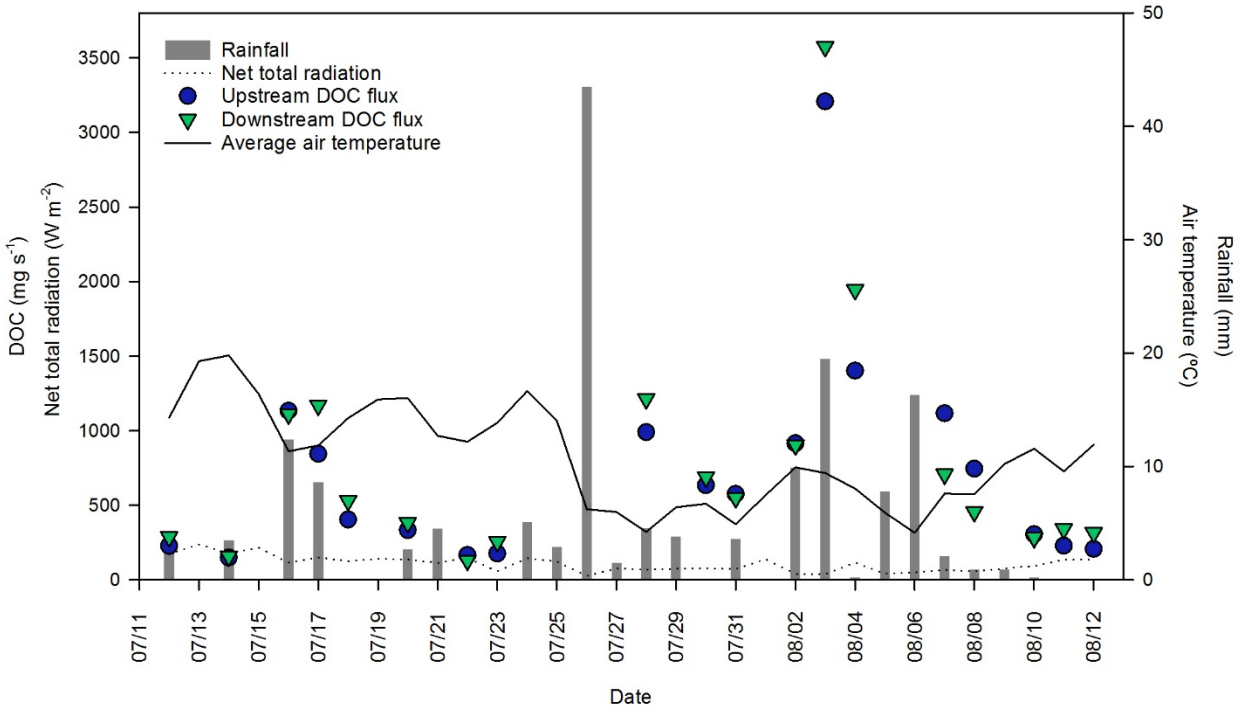

Fig. 6: Environmental conditions (solar radiation, precipitation and mean daily air temperature) and DOC flux upstream and downstream of slump FM3 across a month-long sample period (July 12-August 12, 2014). Corresponding multiple linear regressions are described in Table 4.

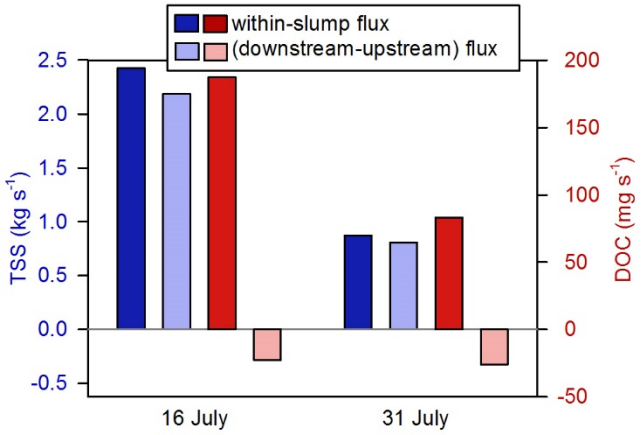

Fig. 7: Within-slump fluxes of dissolved organic carbon (DOC), and TSS, compared to the calculated (downstream - upstream) fluxes for these two constituents. TSS – a conservative tracer over short distances – shows an additive response where the measured within-slump flux is equivalent to the calculated (downstream - upstream) flux. In contrast, DOC shows clear evidence of downstream loss.

1058